MODELING AND SIMULATION OF CO_2-RICH SYNTHESIS GAS TO DIMETHYL ETHER CONVERSION IN MICROCHANNEL REACTORS

by

Uğurcan Tozar

B.S., Chemical Engineering, Ege University, 2015

Submitted to the Institute for Graduate Studies in
Science and Engineering in partial fulfillment of
the requirements for the degree of
Master of Science

Graduate Program in Chemical Engineering

Boğaziçi University

2019

ACKNOWLEDGEMENTS

First of all, I would like to thank my thesis supervisor Prof. Ahmet Kerim Avcı for his support during this study.

Besides my advisor, I would also like to thank Prof. Hüsnü Atakül and Assoc. Prof. A. Kerem Uğuz, my thesis committee for allocating their valuable time, their encouragement, insightful comments on my study.

I sincerely admire the contribution of all my lab friends in KB-404; Sinan Koç, Selin Baç Bilgi, Furkan Öztürk, Mert Özden, Necdet Semih Altinsoy, Özge Selçuk, Hasan Köybaşı, Ceren Hatipoğlu. Besides, I would like to express my deepest appreciation to all my beloved friends who render each day in KB more enjoyable, especially Seymen İlke Kaykanat, Merve Yüce, Ezgi Öztürk, Batuhan Altıntaş, Ahmet Coşgun, Pınar Eribol, Cihat Öztepe, Merve Eropak, Ali Uzun, Olcay Türkmen, Burcu Oral, Nejat İbrahimov, Gülten Çelebi, Ekin Yurdakul, Deniz Köse, Onur Boy, Elif Esvap, Barış Demirci, Aykübe Leba, İpek Paksoy, Pınar Özdemir and Çağla Odabaşı Özer. They have never left me alone during the difficult times of this research.

I want to thank my close friends other than KB-life, Yasin Dalmaz and Halil Can Göktay for their endless support.

I would like to acknowledge the guidance and support of all of my professors and supporting personnel of chemical engineering department.

Last but not least, I am especially grateful to my family for their endless patience and support during my life. I am so lucky to have them.

The financial support is provided by TUBİTAK through project no: 118M518.

ABSTRACT

MODELING AND SIMULATION OF CO_2-RICH SYNTHESIS GAS TO DIMETHYL ETHER CONVERSION IN MICROCHANNEL REACTORS

Dimethyl ether (DME) is considered as a strong counterpart of oil derivative fuels, such as liquid petroleum gas (LPG) and diesel fuel, due to its environmentally friendly combustion characteristics and compatibility with existing infrastructure. This study aims model based comparison of two wall–coated microchannel reactors on the basis of conversion of syngas composed of H_2, CO and CO_2, and yield of DME. In the first configuration,namely the mixed bed, 1:1 (by mass) physically mixed, porous layers of Cu–ZnO/Al_2O_3 and γ–Al_2O_3, synthesis and dehydration catalysts, respectively, are considered to be washcoated to the opposing faces of the rectangular shaped microchannel, whereas separate layers of Cu–ZnO/Al_2O_3 and γ–Al_2O_3 face each other in the second configuration, namely the opposing bed. Comparisons are carried out at inlet pressure, temperature, molar H_2/CO and H_2/CO_2 ratio ranges of 20–60 bar, 493–508 K, 2.5–4.0 and 5–12, respectively, under identical contact times. On both configurations, fast temperature rise ($\sim<8$ K) at the channel entrance is observed, subsequently decreases along the reactor owing to in situ heat removal of integrated air cooling. Higher DME yield ($\sim$3.2%) and CO_2 ($\sim$10.5%) conversion are obtained on the opposing bed, whereas elevated CO conversion ($\sim$60%), is observed on the mixed bed. Negative CO_2 conversions dictated by excess methanol produced by faster CO hydrogenation, observed on the mixed bed, is hampered on the opposing bed. Two dimensional steady–state modeling of the reactors is based on conservation of momentum and species mass together reactive transport within the wash-coated porous catalyst layer, all of which are solved by the finite volume method run under ANSYS-Fluent software.

ÖZET

MIKROKANAL REAKTÖRLERDE CO_2 İÇERİKLİ SENTEZ GAZININ DİMETİL ETERE DÖNÜŞÜMÜN MODELLENMESİ VE BENZETİLMESİ

Dimetil eter çevre dostu yanma özelliği ve mevcut altyapıya uyumluluğu nedeniyle petrol türevi yakıtların en güçlü rakibi olarak gösterilmektedir. Bu çalışmada, H_2, CO ve CO_2'den oluşan sentez gazı dönüşümü, metanol ve DME verimlerine dayanarak iki duvar kaplı mikrokanal reaktör modelinin karşılaştırılması amaçlanmaktadır. Birinci konfigürasyonda, kütlece 1:1 fiziksel olarak karıştırılmış Cu–ZnO/Al_2O_3 ve γ–Al_2O_3, sırasıyla metanol sentez ve bozunma katalizörleri, gözenekli tabaklaraının dikdörtgen şeklindeki mikrokanalın karşıt yüzeylerine kaplanmış olduğu kabul edilirken ikinci konfigürasyonda ayrı Cu–ZnO/Al_2O_3 ve γ–Al_2O_3 katalizör tabakaları karşılıklı yerleştirilmektedir. Karşılaştırmalar aynı temas süreleri altında, giriş basıncı, sıcaklık, molar H_2/CO ve H_2/CO_2 oranı, sırasıyla, 20–60 bar, 493–508 K, 2,5–4 ve 5–12 aralığında gerçekleştirilmektedir. Her iki konfigürasyonda, kanal girişlerinde en fazla 8 K'lik sıcaklık artışı ve akabinde sisteme entegre edilen hava soğutması sayesinde kanal boyunca sıcaklıkda düşüş gözlemlenmektdir. Karşılıklı yatakta daha yüksek DME verimi ($\sim$%3.2) ve CO_2 dönüşümü ($\sim$%10.5) elde edilirken, karışık yatakta yüksek CO dönüşümü ($\sim$%60) gözlemlenmektedir. Karışık yatakta gözlemlenen daha hızlı CO hidrojenasyonu ile üretilen fazla metanol tarafından dikte edilen negatif CO_2 dönüşümleri karşı yatakta engellenmektedir. Reaktörlerin iki boyutlu kararlı modellenmesi, maddelerin gözenekli katalizör tabakası içerisindeki momentum ve kütle korunumlarının reaksiyon iletimleriyle beraber ANSYS-Fluent yazılımında sonlu hacim methodu kullanılarak çözülmesine dayanmaktadır.

TABLE OF CONTENTS

LIST OF FIGURES

LIST OF TABLES

LIST OF SYMBOLS

C_2	Inertial resistance coefficient of the washcoat (m^{-1})
cat	Catalyst
$c_{p,m}$	Heat capacity of gas mixture (J kg^{-1} K^{-1})
$D_{eff,i,m}$	Effective diffusivity of species i in the mixture, (m^2 s^{-1})
$D_{i,m}$	Diffusivity of species i in the mixture, (m^2 s^{-1})
$d_{particle}$	Particle diameter (m)
eff	Effective
f_i	Fugacity of species i in the mixture (bar)
$f_{pure,i}$	Fugacity of pure species i (bar)
$\vec{\mathbf{F}}$	Momentum source/sink term (kg m^{-2} s^{-2})
$G_{f,i}$	Gibbs free energy of formation of species i (kJ mol^{-1})
$H_{f,i}$	Enthalpy of formation of species i (kJ mol^{-1})
$\mathbf{I}$	3x3 identity matrix
i	Species indices
$\vec{J_i}$	Diffusive mass flux of species i (kg m^{-2} s^{-1})
$K_{D,rxn}$	Reaction equilibrium constant (MS1 and MS2; bar^{-2}, MD; -)
K_i	Adsorption/desorption equilibrium constant for species i (bar^{-1})
$k_{eff,m}$	Effective thermal conductivity of gas mixture in the washcoat layer (W m^{-1} K^{-1})
k_{rxn}	Reaction rate constant (MS1; kmol m^{-3} s^{-1} bar^{-3}, MS2; kmol m^{-3} s^{-1} bar^{-4}, MD; kmol m^{-3} s^{-1} bar^{-1})
k_m	Thermal conductivity of gas mixture (W m^{-1} K^{-1})
k_w	Thermal conductivity of the solid wall (W m^{-1} K^{-1})
L	Microchannel length (m)
m	Mixture
M_i	Molecular weight of species i (kg mol^{-1})
n_i	Number of moles of species i (mol)
Nu	Nusselt number

P	Total pressure (bar)
p	Particle
r_{rxn}	rate of reaction (MS1, MS2, MD; kmol m^{-3} s^{-1})
R	Gas constant (=8.314 J mol^{-1} K^{-1})
R_i	Consumption/generation rate of species i (kmol m^{-3} s^{-1})
Re	Reynolds number
rxn	Reaction
$S_{f,i}$	Entropy of formation of species i (kJ mol^{-1} K^{-1})
Sh	Sherwood number
T	Temperature (K)
$\vec{\mathbf{v}}$	Velocity vector (m s^{-2})
w	Solid wall phase
x, y, z	Cartesian coordinates
y_i	Mole fraction of species i
Y_i	Mass fraction of species i
α	Permeability of the washcoat (m^2)
ΔG_{rxn}	Gibbs free energy of reaction (MS1, MS2, MD; kJ mol^{-1})
ΔH^o	Standard enthalpy of reaction (kJ mol^{-1})
ΔH_{rxn}	Enthalpy of reaction (MS1, MS2, MD; kJ mol^{-1})
ϵ_{cat}	Porosity of the washcoat layer
μ_i	Viscosity of species i, (kg m^{-1} s^{-1})
μ_m	Average gas mixture viscosity, (kg m^{-1} s^{-1})
ρ_m	Density of gas mixture, (kg m^{-3})

LIST OF ACRONYMS/ABBREVIATIONS

1D	One dimensional
2D	Two dimensional
3D	Three dimensional
CH_3OH	Methanol
CH_3OCH_3	Dimethyl ether
CH_4	Methane
CO	Carbon monoxide
CO_2	Carbon dioxide
CWP-Cu–ZnO/Al_2O_3	Catalyst washcoated phase of CZA
CWP-γ–Al_2O_3	Catalyst washcoated phase of dehydration catalyst
CZA	Cupper-Zinc oxide-Alumina
DME	Dimethyl ether
FP	Fluid phase
H_2	Hydrogen
H_2O	Water/steam
HZSM-5	Zeolite socony mobil no. 5
LPG	Liquified petroleum gas
MS1	Methanol synthesis from carbon monoxide
MS2	Methanol synthesis from carbon dioxide
MD	Methanol dehydration
MW	Molecular weight
N_2	Nitrogen
NO_x	Nitrogen oxides
RWGS	Reverse water-gas shift
STD	Syngas-to-DME
WGS	Water-gas shift

1. INTRODUCTION

Energy means ability to do a work. A number of energy forms exist in the earth. Those are chemical, electrical, thermal, radiant, light, mechanical and nuclear energy [12]. World energy demand is increasing with an immense growth year by year due to increasing population which is from 1.6 billion to 7.3 billion within the last century. Fossil fuels are considered the major energy source and fuels derived from this source are an irreplaceable parts of world economy [13]. The primary source among those fossil fuels is considered as oil. However, oil is not an unlimited and renewable source, furthermore world oil reserve is not predicted [1]. However, both increasing population and environmental damage caused by fossil fuels have led governments and industries to seek alternative ways, such as renewable energy resources. Share of renewable fuels production among the other energy sources have been rising and it is going to increase in the following decades [14].

Renewable fuel resources are considered environmentally friendly energy that is pollution free. In other words, they do not cause the production of hazardous waste when used. Therefore, any other fuels converted from fossil fuels or waste products are not considered in those group [15].

Biomass is a terminology identified the earth materials which have photosynthesis ability, such as plants and crops. Those organic materials are turned into energy, called bioenergy [15]. Although biomass is sustainable and environmentally friendly, it has various common characteristic property with fossil fuels. Biomass is converted into biofuels (gas and liquid) which can be easily transported wherever it is needed. Besides its conversion characteristics, it can be used as an energy source as a result of its combustion process. Bioenergy is obtained from biomass by applying several ways, such as gasification, combustion, reforming and pyrolysis [15]. Dimethyl ether is considered one of the most crucial fuels which is obtained from biofuels. DME is an attractive fuel with its safe transportation and environmentally friendly combustion characteristics (CO and NO_x free) when it is compared to petroleum derivatives (i.e.

diesel and LPG) [1].

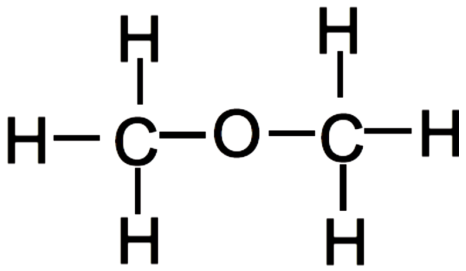

Figure 1.1. Molecular structure of DME [1].

DME is in liquid phase above 5 bar and it has high volatility. A visible blue flame, which is the same combustion characteristics of butane and propane, is observed when it is burned. It can be used for domestic use as a strong candidate for replacing LPG. As opposed to LPG, DME is known as an environmentally friendly fuel. The molecular structure of DME consists of C-H and C-O bonds, it has no direct C-C bond (Figure 1.1). 35% of one DME molecule is oxygen. Moreover, CO amount obtained by DME combustion is in a lower level than those of natural gas [9]. High cetane number (above 55) indicates that DME is a forceful counterpart of petroleum derivatives [1]. Due to the fact that vapor pressure of LPG and DME are identical,therefore DME can be easily adapted to existing infrastructure [9].

Table 1.1. Physical properties of DME [9].

Properties	
Molecular formula	C_2H_6O
Molar mass	46.07 g mol^{-1}
Appearance	Colorless gas
Density	0.735 g mL^{-1}
Melting point	-141 ^oC
Boiling point	-24 ^oC
Vapor pressure	1.5 bar

Feedstock used in DME synthesis is synthesis gas which consists of mostly CO, H_2, CO_2. Synthesis gas is derived from biomass by means of either gasification or reforming processes [16]. Two production methods are used to obtain DME, namely direct and indirect routes. In the conventional method (indirect route), methanol, an intermediate product occurs previous step of DME synthesis, is produced from synthesis gas over a metal catalyst in the first reactor (Reactions 2.1 and 2.2) and then, methanol is conveyed to second reactor to be converted into dimethyl ether over an acidic catalyst [9, 17, 18]. The methanol synthesis reactor have to be pressurized in a range of 50 and 150 bar due to thermodynamically limited methanol formation reaction [17]. In the direct route, on the contrary, methanol synthesis and dehydration reactions (Reactions 2.1-2.3) take place on mechanical mixing of methanol synthesis and dehydration (hybrid or bifunctional) catalysts packed in a single reactor [3]. Suggested operating condition for commercial Cu–ZnO/Al_2O_3 and γ–Al_2O_3 catalyst mixing is in a range of 498-573 K and 10-50 bar [17]. Thermodynamic limitation of syngas to methanol, encountered in conventional method, is hampered on hybrid catalyst and this exceeds syngas conversion. Therefore, direct route is more attractive than conventional method [2].

Direct synthesis method is more advantageous than conventional route from economical point of view. Methanol synthesis and subsequent dehydration in a single reactor allows more effective syngas conversion and decreases design costs [9]. Methanol obtained from the first reactor, in indirect method, is needed to be purified before to be fed to second reactor and this rises operational costs as well [18].

Temperature control plays a significant role on direct DME synthesis to optimize syngas conversion and DME yield. Combining all exothermic reactions (Reactions 2.1-2.3) inside a one-single reactor brings together abrupt temperature hot-spot formation which may cause to local catalyst deactivation [19]. In a conventional packed bed reactor with integrated cooling, reaction temperature attains $\sim$40 K divergence with respect to inlet temperature (Figure 1.2). Methanol synthesis and dehydration reaction steps are in thermodynamically and kinetically equilibrium which can be negatively influenced by a temperature run-away. In the frame of effective temperature control,

microchannel (microstructured) reactor technology draws attention owing to its high heat and mass transfer rates which may improve process efficiency [20]. Microchannel reactors are shaped by parallelly located channels, which have dimension between 10^{-6} and 10^{-3} m, separated by solid metal walls and operated in laminar flow conditions [21]. Porous catalyst is washcoated to the both side of the channel walls. Surface to volume ratio of a microchannel reactor is much higher, up to 10^3 times, than a conventional packed bed reactor. Efficient conductivity of constructing material and having high surface to volume ratio provide a convenience to microchannel reactors upon constructing nearly isothermal conditions while processing exothermic reactions, i.e. DME synthesis [22].

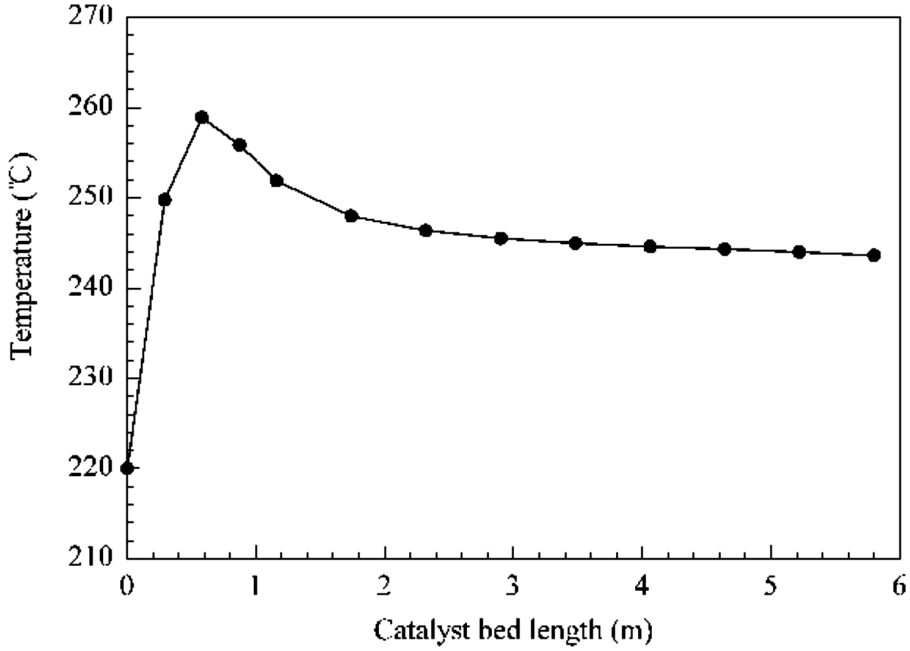

Figure 1.2. Temperature distribution a conventional fixed bed reactor with integrated cooling [2].

In this work, it is aimed to compare syngas conversion and DME synthesis performance of two wall coated microchannel reactor geometries in terms of catalyst layer configurations, namely the mixed bed and the opposing bed, by changing inlet temperature, inlet pressure, inlet molar flow rate ratios of H_2/CO and H_2/CO_2. The constructed models are validated by experimental data acquired from literature [2].

This thesis contains 5 main chapters. In chapter 2, a comprehensive literature survey is presented. In chapter 3, the mathematical modeling of two microchannel reactor systems, reaction kinetics regarded to reaction network system, and operational parameters are explained. In chapter 4, effect of changing parameters on both reactor configurations are investigated. In final, chapter 5, research is concluded and some recommendations are presented regarding future studies.

2. LITERATURE SURVEY

2.1. Microchannel Reactor

Growing technological advancements contribute decreasing reactor volume using micromachining techniques [23]. A catalytic microchannel reactor consists of subsequent parallelly constructed channels which have hydraulic diameter in sub-millimetre range [24]. Minimalized and parallized construction provide many advantages in the context of process efficiency and safety [3].

Microstructured reactor technology in chemical processes is considered as a breakthrough in the context of process intensification. The parallel blocks are constructed with hydraulic diameter in a range of 10^{-6}-10^{-3} m. Owing to narrower channel diameter, fluid flow is operated in laminar regime. Heterogeneous reactions take place on thin catalyst layer coated to the inner side of the channel walls made up metallic materials,such as stainless-steel. As a result of washcoated thin catalyst layer, heat and mass transfer resistances, which encountering in a typical conventional reactor, is not observed in a microchannel reactor [25]. Moreover, lower level of pressure drop due to high channel porosity (<0.8) is another valuable asset of these units [21]. Surface to volume ratios are in a range of 10^4-10^5 m^2/m^3, whereas, it is calculated as 10^3 in their conventional competitors [21]. In microstructured geometries, coating catalyst layer to the solid metallic wall provides to both attaining high heat transfer rate and efficient catalyst usage [25].

Integrating heat exchange system to a microchannel reactor geometry plays a significant role in process intensification due to high heat transfer capability arising from both construction material and coated catalyst layer [21]. Bac *et al.* [26] investigated ethylene oxide synthesis in a wall-coated heat exchange enabled microchannel reactor. Ethylene oxide synthesis is conducted by stiff exothermic reaction network. In the case of adiabatic operation, channel temperature gradient approximately attained 50 K, whereas, nearly isothermal condition can be satisfied by enabling counter-current

air cooling as simultaneous heat removing from the system.

Hayer *et al.* [3] conducted both an experimental and a simulation study regarding direct DME synthesis in a heat exchange integrated microchannel reactor over bifunctional catalyst. Reactor model was constructed in 2D geometry to compute temperature and concentration gradients in accurate way. Calculations made using COMSOL Multiphysics software. Effect of temperature, pressure, space velocity of syngas and inlet molar ratio of CO in syngas feed on reactor performance were investigated. Sufficient heat removing capacity provided nearly isothermal conditions. Temperature divergence was above 2 K. This gradient was computed on a conventional fixed bed reactor operated under the same conditions with the microchannel as 40 K (2.1).

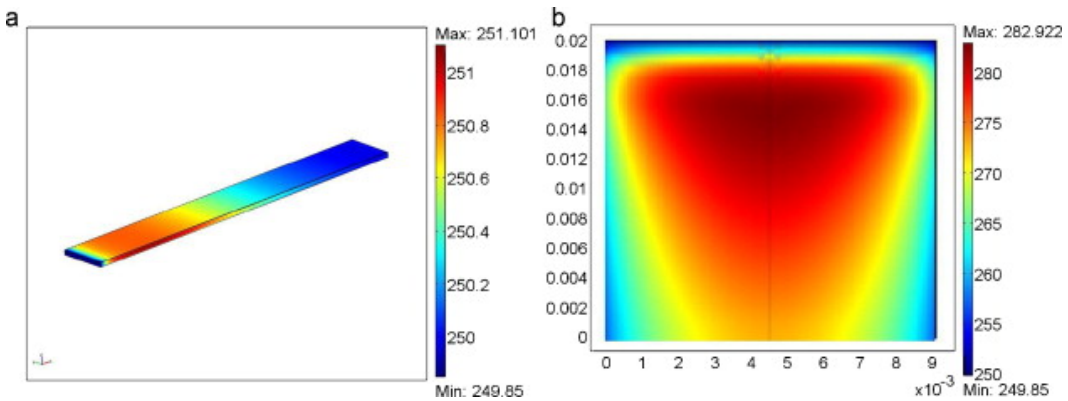

Figure 2.1. (a) heat distribution in the microchannel reactor, (b) heat distribution in a conventional fixed-bed reactor operating under the same conditions with the microchannel [3].

Microchannel reactors are promising units due to advantageous heat and mass transfer capabilities which is also significant in direct DME synthesis comprised of thermodynamically equilibrium reactions [3]. Not only low syngas conversion and DME yield but also catalyst deactivation arise from uncontrolled temperature run-away [9].

2.2. DME Synthesis

DME production is divided into two categories, namely single step and two step. In two-step synthesis (conventional method), methanol is produced from syngas over a metal-copper based catalyst, i.e. Cu–ZnO/Al_2O_3, in the first reactor. And then, methanol is converted into DME over an acid catalyst i.e. γ–Al_2O_3 or HZSM-5. This route is also named indirect DME synthesis [27]. Syngas hydrogenation is thermodynamically limited due to stiff temperature rising in the reaction medium [28]. On the other hand, by combining methanol synthesis and dehydration reaction in a single reactor to take place over a hybrid (bifunctional) catalyst, formed by mechanical mixture of synthesis and dehydration catalysts, is called direct synthesis route. Thermodynamic limitation of syngas conversion to methanol is hindered by simultaneous conversion of methanol to DME, while doing so, CO conversion is also accelerated [23]. Syngas consisted of homogeneous gas mixture of CO, H_2 and CO_2 is converted into DME by following reaction steps:

$$\text{Methanol synthesis 1 (MS1): } CO + 2H_2 \rightleftharpoons CH_3OH \qquad \Delta H^0 = -90.4 \text{ kJ mol}^{-1} \quad (2.1)$$

$$\text{Methanol synthesis 2 (MS2): } CO_2 + 3H_2 \rightleftharpoons CH_3OH + H_2O \qquad \Delta H^0 = -49.4 \text{ kJ mol}^{-1} \quad (2.2)$$

$$\text{Methanol dehydration (MD): } 2CH_3OH \rightleftharpoons CH_3OCH_3 + H_2O \qquad \Delta H^0 = -23.0 \text{ kJ mol}^{-1} \quad (2.3)$$

Reverse water-gas shift (RWGS) effect depends on CO_2 amount in the feed stream and it becomes in equilibrium as soon as syngas meets fresh catalyst layer [29]:

$$CO_2 + H_2 \rightleftharpoons CO + H_2O \qquad \Delta H^0 = 41.0 \text{ kJ mol}^{-1} \quad (2.4)$$

Exothermicity of Reactions 2.1-2.3 lead to boost reaction temperature and methane formation is observed above 573 K [30]:

$$CO + 3H_2 \rightleftharpoons CH_4 + H_2O \qquad \Delta H^0 = -206.0 \text{ kJ mol}^{-1} \tag{2.5}$$

2.2.1. Indirect DME Synthesis

DME is conventionally produced from syngas by two step process. Reaction 2.1 and 2.2 occur over commercial Cu–ZnO/Al_2O_3 (under 50-100 bar pressure and 493-553 K temperature) and purified methanol is dehydrated to DME in the second reactor packed with an acid catalyst (mostly γ–Al_2O_3) under ambient conditions due to the fact that Reaction 2.3 is in stoichiometric balance [4]. The schematic representation of conventional route is presented in Figure 2.2.

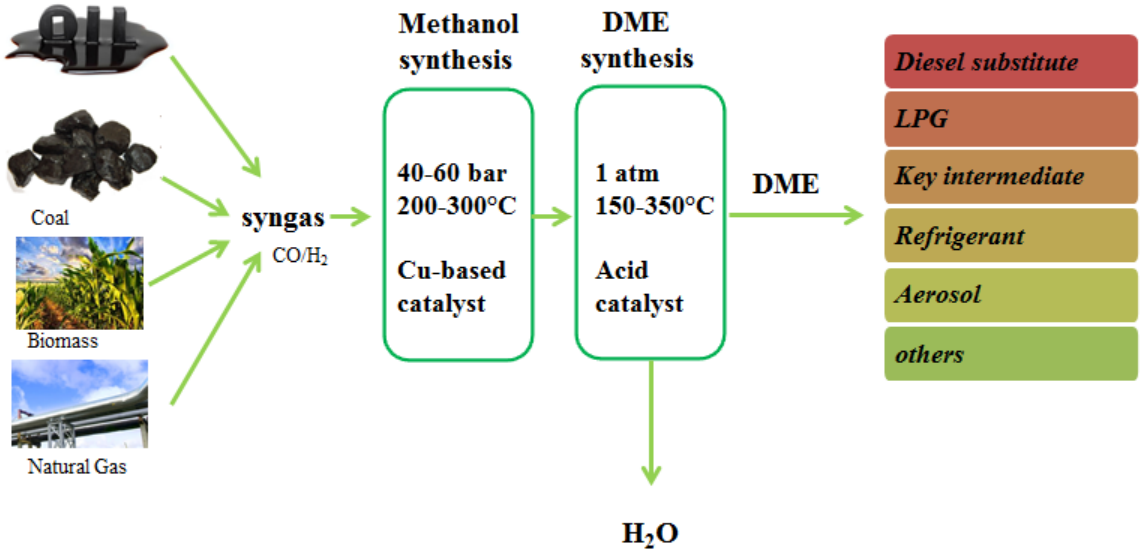

Figure 2.2. Description of indirect DME synthesis method [4].

Kinetic studies regarding DME synthesis from methanol have been reported as either either Langmuir–Hinshelwood or Eley–Rideal reaction kinetic network equations [31, 32], DME and H_2O is contained as inhibitor in both kinetic model definitions [33].

Raoof *et al.* [34] investigated operating temperature effect on methanol dehydration to DME synthesis. A heterogeneous packed bed reactor filled with γ–Al_2O_3 and bed temperature was changed a range of 506 and 576 K. Reactor was operated under adiabatic condition. Methanol conversion increased from 28% to 85% by changing temperature in operational range. Catalyst deactivation period was investigated by adding water to pure methanol feed. It was revealed that steam in the feed stream had a negative impact on methanol dehydration catalyst (γ–Al_2O_3).

Zeolite catalysts constitute as an alternative of commercial γ–Al_2O_3 in methanol-to-DME conversion reactions [27]. Rownaghi *et al.* [35] conducted a series of experiments using ZSM-5 zeolite as methanol dehydration catalyst in different crystal sizes, namely nano, mezo and con with an increasing order. A fixed bed reactor was operated under 1.1 bar pressure and temperature range of 453-593 K. The highest methanol conversion was observed on nano-ZSM-5 catalyst due to absence of heat and mass transfer resistance arising from particle size. The lowest conversion, on the other hand, observed on con-ZSM-5 (the biggest crystal size). DME yield was also enhanced by decreasing particle size and increasing temperature.

Zhu *et al.* [36] performed an experimental study regarding two step DME synthesis in a fixed bed reactor, divided into two stages as top (methanol synthesis) and bottom (methanol dehydration) and packed with Cu–ZnO/Al_2O_3 and HZSM-5 catalysts, respectively. Detailed schematic representation of experimental set-up can be found elsewhere [36]. The influence of syngas (H_2 and CO) pressure, temperature, H_2/CO ratio and space velocity on reactor performance in terms of CO conversion and DME yield was investigated. Reactor was efficiently operated in temperature range of 543-553 K and 508-518 K for the top and bottom section, respectively. The highest CO conversion observed by adjusting H_2/CO ratio as 2. Optimum space velocity was reported in the range of 1000-1300 h^{-1}. Both synthesis and dehydration catalyst was tested under 8 MPa pressure, H_2/CO ratio of 2, the space velocity of 1800 h^{-1}, 541 K for the top and 509 K for the bottom section temperature and remained stable over 100 h.

Membrane are used as selective barriers or play a significant role in chemical processes [9]. Catalytic membrane reactors contribute to product improvement by accelerating reactions in equilibrium. Membrane reactors allow in situ separation while reaction takes place on catalyst [5]. H_2O formation resulted from methanol dehydrogenation in indirect DME synthesis can be hindered by removing undesired steam, decreased catalytic activity, from reaction environment through membrane [9]. Samimi *et al.* [5] developed a mathematical model included membrane integrated spherical packed bed reactor to dehydrate methanol. Reaction took place over γ–Al_2O_3 catalyst under 18.18 bar pressure and in the temperature range of 495-550 K. Inner side of the sphere was coated by water selective membrane, which is called H-SOD. Control volume of membrane integrated spherical fixed bed reactor is illustrated in Figure 2.3. In situ water removal from reaction environment accelerated methanol dehydration both thermodynamically and kinetically. Ordinary differential equations were solved under MATLAB software using backward finite difference method. Comparison between conventional packed bed and membrane integrated spherical packed reactor has been made and proposed model achieved higher DME yield with a difference of 13%. Moreover, lower pressure drop was calculated on proposed model than the conventional packed bed reactor.

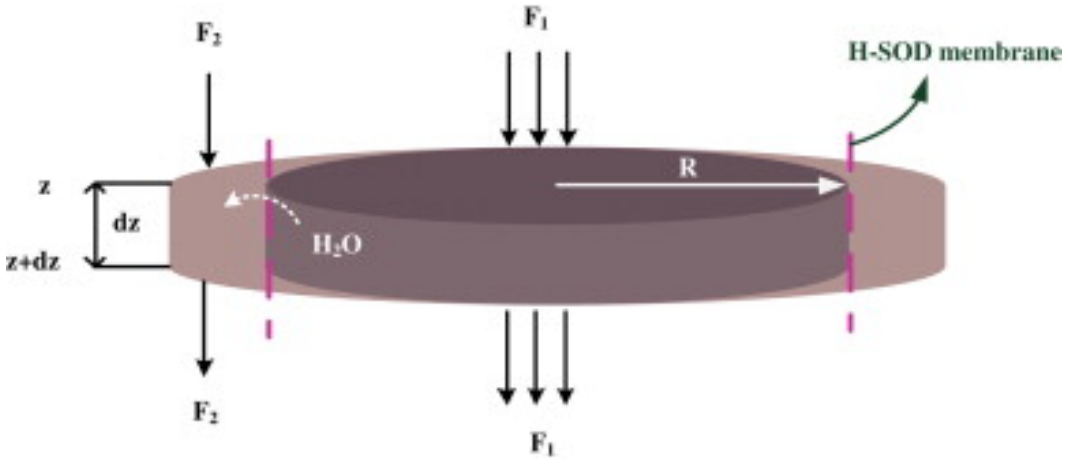

Figure 2.3. Control volume description of membrane integrated reactor [5].

2.2.2. Direct DME Synthesis

Direct synthesis method has been emerged as a novel way of DME production [27]. Syngas gas feed is converted to methanol and subsequently turned into DME over a bifunctional (hybrid) catalyst prepared by combining synthesis and dehydration catalysts to each other using physical methods [9]. Thermodynamic limitation of methanol synthesis reaction is hindered by in-situ methanol conversion. Moreover, the cost of methanol purification, high pressure needed for methanol synthesis from syngas and sophisticated reactor design is prevented applying one-step production method [3].

The performance of different DME synthesis catalyst types have been investigating to improve efficiency of direct synthesis method [9]. The most used hybrid catalyst is the combination of Cu–ZnO/Al_2O_3 (CZA) and γ–Al_2O_3 catalysts [27]. In many studies [6, 30, 37, 38], CO conversion (∼53-95%) and DME yield (∼34-52%) over CZA mixture of γ-Al_2O_3 were elevated when temperature was risen from 513 K to 563 K, while doing so H_2/CO ratio and pressure was remained constant at the values of 2 and 50 bar, respectively. Jia *et al.* [39] researched the effect of methanol dehydration catalyst amount in the bifunctional catalyst mixture on the syngas conversion. In γ-Al_2O_3-free conditions, CO conversion was observed ∼22%. When 0.2 g dehydration catalyst was added to CZA, which was kept constant as 4 g, CO conversion was remarkably risen up to ∼47%.

Water and coke formation in the reaction medium leads to deactivation of alumina origin catalyst. Moreover, optimum temperature of dehydration reaction which takes place over γ-Al_2O_3 is above the average temperature value required in the methanol synthesis reaction, which occurs on Cu based catalyst, therefore Cu based catalyst is likely to deactivation through sintering [40]. Zeolite based catalysts are drawing attention due to stability and adjustable acidity level [41]. Owing to hydrophobic character, zeolites are distinguished from their counterparts (i.e. γ-Al_2O_3) by demonstrating catalytic activity at lower reaction medium temperatures where CO hydrogenation reaction (2.1) is thermodynamically promoted [42–44].

Amount of catalyst in mixture is a crucial parameter which affects product distribution, such as syngas conversion and DME yield. Pelaez *et al.* [17] investigated the optimum weights of methanol synthesis (Cu–ZnO/Al_2O_3) and dehydration (γ-Al_2O_3) catalysts in a hybrid mixture by constructing isothermal fixed-bed reactor model. Optimum weight percentage of Cu based catalyst and acidic catalysts were computed as 92.5% and 7.5%, respectively. Moreover, it was indicated that presence of CO_2 in the feed stream was found to be significant in terms of reaction kinetics and water-gas shift reaction was at equilibrium along the reactor.

Immense heat generated by STD reactions lead to many undesirable impacts on not only catalyst activity but also product distribution, therefore kinetically and thermodynamically reversible reaction network equations have to be avoided uncontrolled thermal run-away [9]. A number of studies have been conducted to regulate temperature rise in the reactor systems [2,8,45,46]. Reactors are designed on the basis functional flexibility are considered such a novel way of process intensification [46]. Vakili *et al.* [18] designed a novel heat exchange integrated reactor configuration in terms of functional flexibility. CO_2 containing syngas conversion by direct route simulated in a steady state 1D heterogeneous fixed-bed reactor model. Heat generated by DME synthesis reactions (Eqs. 2.1-2.3), where took place over equally mixed of Cu–ZnO/Al_2O_3 and γ-Al_2O_3, was removed by endothermic cyclohexane dehydrogenation, where took place over Pt/Al_2O_3, in the adjacent tube. The amount of produced DME was approximately improved as 600 ton/year by proposed model.

Besides fixed-bed reactors, slurry reactors play a key role in commercial direct DME production [47]. Solvent suspends the catalyst and syngas is distributed as bubble form in this solvent. Achieving efficient heat transfer rates and lower investment cost make slurry reactors an attractive process unit for the large scale operations [18]. Temperature control in slurry phase reactors are much more adjustable than their conventional counterparts (i.e. fixed-bed reactors) [48]. Papari *et al.* constructed a 1D steady-state mathematical model to simulate direct DME synthesis from syngas, containing CO_2, in a three-phase slurry reactor. A schematic representation of the slurry column reactor model is presented in Figure 2.4. Reactor was operated under

isothermal and non-isothermal conditions and there was no found a difference between those two operating conditions. It was also indicated that reactor performance in terms of CO conversion and DME yield attained optimum value at 533 K and 50 bar.

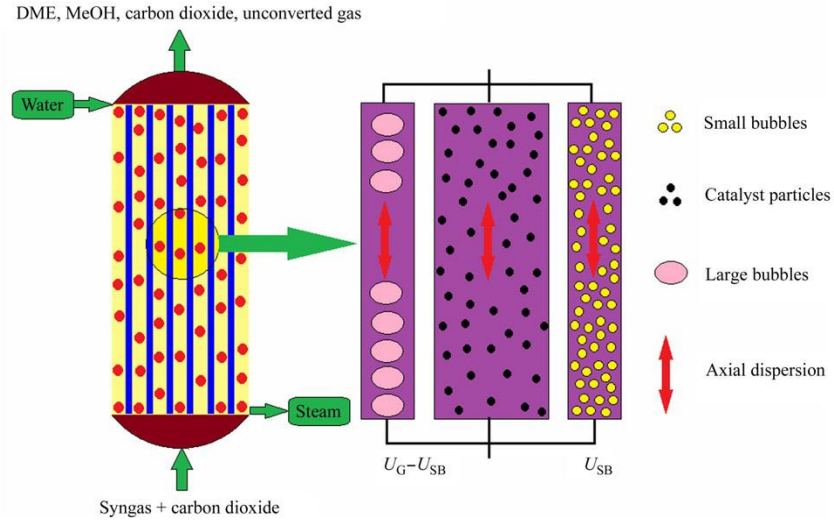

Figure 2.4. Slurry column reactor [6].

CO/CO_2 ratio in feed stream is considered a significant variable in direct DME synthesis. In CO-rich conditions, steam formation, as a result of methanol dehydration, is hampered by the activity of WGS Reaction 2.4) [23]. On the other hand, CO_2-rich conditions promote excess methanol formation owing to large amount of H_2O generated in CO_2 hydrogenation and methanol dehydration reactions. Therefore, DME formation is hindered. In situ steam removal from reaction environment positively affects DME formation [37]. Iliuta *et al.* [7] developed an unsteady-state 1D mathematical model to model a dual bed reactor configuration in direct syngas conversion to DME. Syngas feedstock was simultaneously obtained from glycerol reforming, which is an endothermic reaction removes heat released by DME synthesis. Methanol synthesis dehydration catalysts were selected as Cu–ZnO/Al_2O_3 and HZSM-5, respectively. Water was discharged by perm-selective membrane located center of the reactor column (Figure 2.5). The proposed model demonstrated the best performance under CO_2-rich conditions and DME formation was promoted by reducing steam. Operational advantage of water selective membrane was investigated by making a comparison between

a conventional fixed bed and a membrane integrated fixed bed [49]. CO_2 conversion and DME yield was enhanced by in situ H_2O removal owing to kinetic acceleration of RWGS reaction.

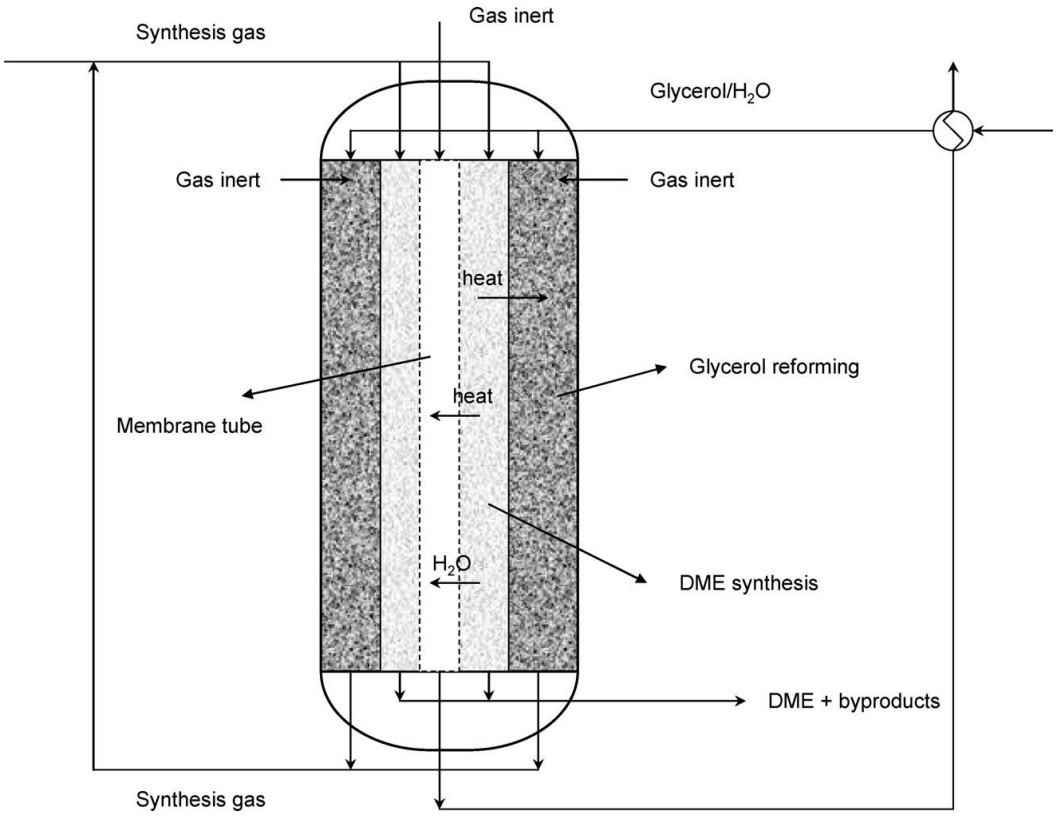

Figure 2.5. Dual bed membrane reactor [7].

Separation processes have a critical role in indirect DME synthesis. Improvements on the basis of distillation separation is made to reduce energy consumption and investments cost. Process intensification come into play when it comes to design economic distillation process. Catalytic distillation draws attention with its attractive properties, such as capital efficiency enhancements, selectivity improvements and energy saving, in the last decade. Catalytic distillation combines reaction and separation in industrial applications, such as DME synthesis. No side product, other than steam, is observed upon catalytic distillation DME synthesis [50].

3. MATHEMATICAL MODELING

3.1. Details of the Microchannel Reactor

Simplified depiction of the heat-exchange integrated microchannel reactor configurations, namely the mixed and the opposing bed, are illustrated in Figure 3.1 and Figure 3.2, respectively. The mixed bed layered reactor unit model consists of, parallelly located, half reaction and cooling channels which are separated from each other by means of a stainless-steel wall. The length and width of the each channel are 7.5×10^{-2} and 6×10^{-4} m, respectively. Besides, height of the reaction and cooling channels, which layered the mixed catalyst block with a thickness of 5×10^{-5} m, are 1.5×10^{-4} m. Cu–ZnO/Al_2O_3 and γ–Al_2O_3 catalyst are physically mixed each other with 1:1 mass ratio and are coated each inner side of the reaction channel with the total weight of 1.07×10^{-5} kg [8].

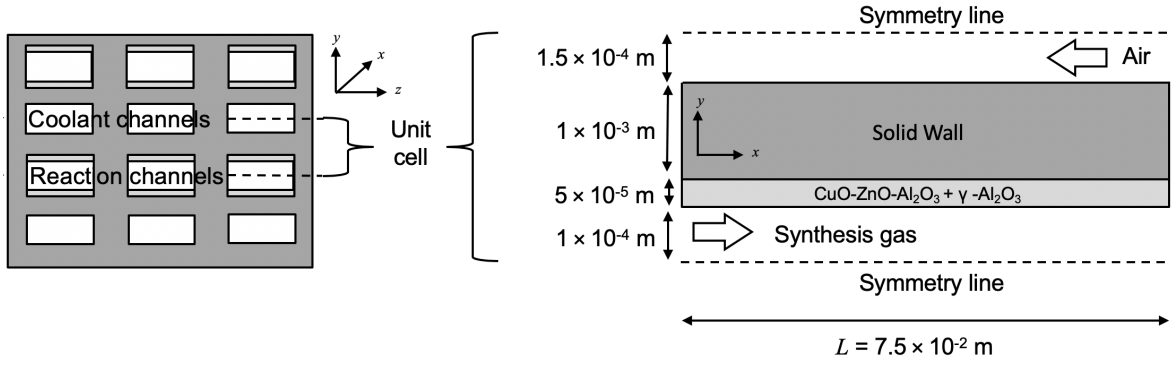

Figure 3.1. Simplified (not to scale) illustrations of the intensified, microchannel DME synthesis reactor (left) and the unit cell (adapted from [8]).

Evolution of Nusselt number (Nu), defined as the ratio of convective heat transfer to conductive heat transfer within the fluid, in ethylene epoxidation which has the same reaction characteristics in terms of heat generation with DME synthesis was investigated in 2D and 3D reactor geometry [45]. It was indicated that there is no significant difference between these dimensions. As a result of this deduction, heat transfer along one dimension (i.e. z-direction) can be neglected.

In the opposing bed, on the other hand, reactor model is composed of one reaction channel and two half of cooling channel, separated by two stainless-steel walls. The length and width of the each channel are 1.7×10^{-1} and 6×10^{-4} m, respectively. Methanol synthesis (Cu–ZnO/Al_2O_3) and dehydration catalyst (γ–Al_2O_3) are coated on the both sides of the reaction channel walls such that facing opposite to each other. Density of Cu–ZnO/Al_2O_3 and γ–Al_2O_3 catalysts are 2366 and 1060 kg m^{-3} [29]. Catalyst amount coated to each side of the channel is equal and the thicknesses are 5×10^{-5} and 2.5×10^{-5} m for dehydration and synthesis catalysts, respectively. For both configurations, the shape of the channels are designed in rectangular form which provides micromachining ease and satisfactory balance between transport and reaction rates due to elevated Nu and Sh numbers in the channels which have smaller hydraulic diameter [24, 51, 52].

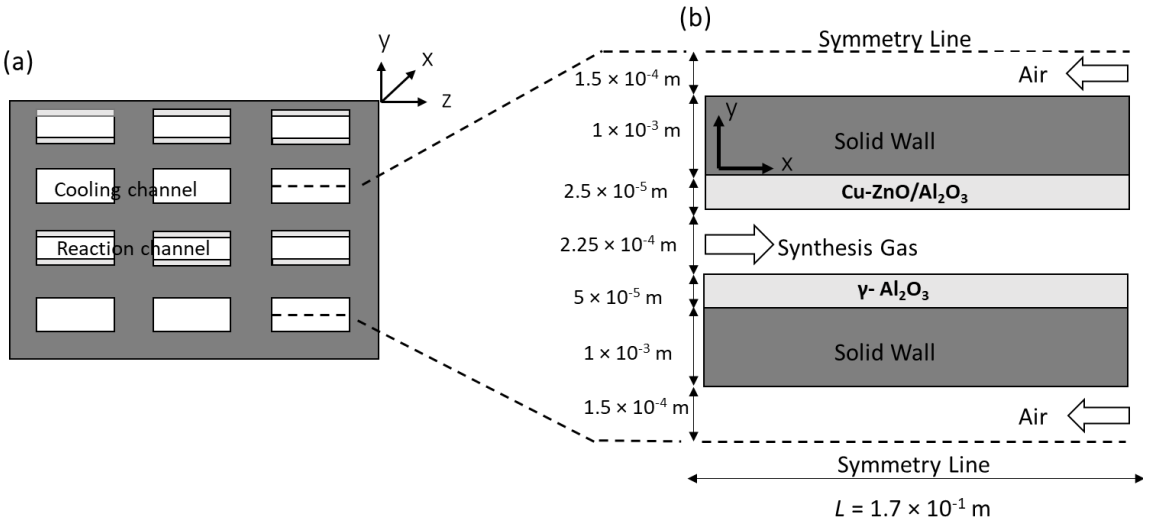

Figure 3.2. Illustrations of the heat–exchange integrated microchannel syngas–to–DME conversion reactor (left) and the unit cell (right). Drawings are not to scale.

3.2. Reaction Network and the Kinetic Model

Dimethyl ether conversion from syngas feedstock consists of simultaneous methanol synthesis and dehydration reactions. Methanol formation is considered only occur on commercial Cu–ZnO/Al_2O_3 catalyst and produced methanol is converted into DME over γ–Al_2O_3 catalyst [2]. In the mixed bed, catalyst are mixed each other (1:1 mass

ratio) by physical methods. In the opposing bed, on the other hand, synthesis and dehydration catalysts are separately washcoated to inner surfaces of the channel. Owing to the fact that RWGS is considered the combination of Reactions 2.1 and 2.2 and is implicitly included in the proposed reaction kinetics, the kinetic information is not included among the reaction network equations. According to literature [53], undesired methane formation (Reaction 2.5) is observed above 573 K, however, temperature of the reaction medium does not exceed the limit owing to integrated counter-current cooling flow. Therefore, Reaction 2.5 is excluded from the model kinetics. Besides, higher temperature values over the limit lead to deactivation of catalyst [19]. Carbon formation represented by reverse Boudouard reaction ($2CO = CO_2 + C(s)$, $\Delta H^0 = -172$ kJ mol^{-1}) is hindered by CO_2 in the inlet stream [19, 54]. On the basis of experimental studies that implied, operated catalysts do not encounter any deactivation issue during operating conditions. In this study, following kinetic model equations which adapted from literature [55] is used for calculating reaction rates of Reactions 2.1, 2.2 and 2.3:

$$r_{MS1} = \frac{k_{MS1} f_{CO} f_{H_2}^2 (1 - \beta_{MS1})}{\left(1 + K_{CO} f_{CO} + K_{CO_2} f_{CO_2} + K_{H_2} f_{H_2}\right)^3}, \quad \beta_{MS1} = \frac{f_{CH_3OH}}{K_{D,MS1} f_{CO} f_{H_2}^2} \tag{3.1}$$

$$r_{MS2} = \frac{k_{MS2} f_{CO_2} f_{H_2}^3 (1 - \beta_{MS2})}{\left(1 + K_{CO} f_{CO} + K_{CO_2} f_{CO_2} + K_{H_2} f_{H_2}\right)^4}, \quad \beta_{MS2} = \frac{f_{CH_3OH} f_{H_2O}}{K_{D,MS2} f_{CO_2} f_{H_2}^3} \tag{3.2}$$

$$r_{MD} = \frac{k_{MD} f_{CH_3OH} (1 - \beta_{MD})}{(1 + \sqrt{K_{CH_3OH} f_{CH_3OH}})^2}, \qquad \beta_{MD} = \frac{f_{CH_3OCH_3} f_{H_2O}}{K_{D,MD} f_{CH_3OH}^2} \tag{3.3}$$

Syngas conversion to methanol reactions (MS1 and MS2) are taken into account only the surface of Cu–ZnO/Al_2O_3 (methanol synthesis catalyst) while methanol dehydration (MD) reaction takes place on γ–Al_2O_3 catalyst [2]. Reaction rate constants and equilibrium constants are defined in Table 3.1 as follows:

Table 3.1. Kinetic model constants [2].

k_{rxn}, K_i=A.exp(B/(RT))	A	B
k_{MS1}	1.2×10^{3}	-43723
k_{MS2}	2.8×10^{1}	-30253
k_{MD}	5.8×10^{1}	-24984
K_{CO}	8.252×10^{-4}	30275
K_{CO_2}	2.1×10^{-3}	31846
K_{H_2}	1.035×10^{-1}	-11139
K_{CH_3OH}	1.726×10^{-4}	60126

Temperature dependent fugacity values of corresponding components existed in the gas mixture is calculated by virial expansion as follows [10]:

$$f_i = y_i f_{pure,i}, \quad f_{pure,i} = exp[(b_i - \frac{a_i}{RT})\frac{p}{RT} + \ln p] \tag{3.4}$$

Predicted reaction equilibrium constants for the Reactions 2.1-2.3 as a function of temperature can be expressed by the following equation:

$$K_{D,rxn} = exp(-\Delta G_{rxn}/RT), \qquad rxn = MS1, MS2, MD \tag{3.5}$$

The coefficients used in the solution methodology of Eqs. 3.1-3.3 and constants related with Gibbs free energy calculations in Eq. 3.8 and 3.9 are presented in Table 3.2 and Table 3.3, respectively.

Table 3.2. The van der Waals coefficients used in calculations of related equations (adapted from [10]).

Species(i)	a_i(bar L^2 mol^{-2})	b_i(L mol^{-1})
CO	1.472	0.03948
H_2	0.2453	0.02651
CO_2	3.658	0.04286
H_2O	5.537	0.03049
CH_3OH	9.472	0.06584
CH_3OCH_3	8.69	0.07742
CH_4	2.3	0.04301

Table 3.3. Gibbs free energy calculation coefficients (adapted from [11]).

Species	a_1	$a_2(\times 10^3)$	$a_3(\times 10^6)$	$a_4(\times 10^9)$	$a_5(\times 10^{12})$	$b_1(\times 10^{-4})$	b_2
CO	3.58	-0.61	1.02	0.91	-0.90	-1.43	3.51
H_2	2.34	7.98	-19.5	20.2	-7.38	-0.092	0.68
CO_2	2.36	8.98	-7.12	2.46	-0.14	-4.84	9.90
H_2O	4.20	-2.04	6.52	-5.49	1.77	-3.03	-0.85
CH_3OH	5.72	-15.2	65.2	-71.1	26.1	-2.56	-1.50
CH_3OCH_3	5.31	-2.14	53.1	-62.3	23.1	-2.40	7.13
CH_4	5.15	-13.7	49.2	-48.5	16.7	-1.02	-4.64

Gibbs free energy of the reaction systems (2.1-2.3) are calculated by taking into account formation enthalpy and entropy of components expressed as a function of temperature.

$$\Delta G_{rxn} = \sum_{i=products} n_i G_{f,i} - \sum_{i=reactants} n_i G_{f,i} \tag{3.6}$$

$$\frac{G_{f,i}}{RT} = \frac{H_{f,i}}{RT} - \frac{S_{f,i}}{R} \tag{3.7}$$

$$\frac{H_{f,i}}{RT} = a_1 + a_2\frac{T}{2} + a_3\frac{T^2}{3} + a_4\frac{T^3}{4} + a_5\frac{T^4}{5} + \frac{b_1}{T} \tag{3.8}$$

$$\frac{S_{f,i}}{R} = a_1\, lnT + a_2T + a_3\frac{T^2}{2} + a_4\frac{T^3}{3} + a_5\frac{T^4}{4} + b_2 \tag{3.9}$$

3.3. Operational Parameters and Numerical Solution Technique

Performance of two microchannel reactor models, namely the mixed and the opposing bed in terms of catalyst layer block, are compared for the different cases, such as inlet temperature, pressure, different molar feed ratios on the basis of H_2/CO and H_2/CO_2. Inlet syngas feed stream homogeneously consists of CO, CO_2, H_2, N_2(inert gas) at 508 K (inlet temperature), 50 bar (inlet pressure), H_2/CO=2.5, H_2/CO_2=10. The range of the investigated operating condition values are 493-508 K for inlet temperature, 20-60 bar for inlet syngas feed pressure, 2.5-4.0 for the ratio of H_2/CO and 5-12 for the ratio of H_2/CO_2. Studied cases are adopted from literature [27]. Cooling fluid temperature and pressure are constant and equal to initial values of syngas for all cases. Constructed material of the reactor wall is selected as stainless-steel with 1×10^{-3} m thickness and this is implied as the most widely used material in well-known micromachining techniques in terms of its reliability and compactness [22]. Parameter influence on reactor model is made by changing each parameter within its particular range while other parameters are kept constant at their base values. Total flow distributed to microchannels is assumed in uniform flow rate and adiabatic system allows to conductive heat transfer by means of metal walls which also indicated as solid boundary condition. Homogeneous flow distribution is considered an important parameter which affects the microreactor performance [56].

On the basis of assumptions above, comparison of two different catalyst layer

blocks are conducted over an predicted model which composed of (i) momentum, heat and mass transfer in the fluid phase, (ii) reaction taken place on porous catalyst layers, (iii) transference of released heat by means of solid wall to cooling channels. All of these mechanisms simultaneously occur in the unit cell sections demonstrated in 3.1 and 3.2. Initial condition of linear syngas velocity is 1×10^{-2} m s^{-1}. This value corresponds with 17540 Nml $gcat^{-1}$ h^{-1} which has the same catalyst weight to flow rate ratio with the similar studies reported in Literature [17, 57]. Inlet coolant flow velocity is adjusted to 10 m s^{-1}, in order to prevent catalyst deactivation which can be arised from hot-spot formation at the channel inlet due to first encountering of syngas with fresh catalyst layer. Air and syngas flow is estimated as Newtonian fluid with Reynolds numbers (Re) $\sim$1.1 and 16, respectively, each of which indicate that flow in the both channels are in laminar. Pressure drop is calculated as less than $\sim$1% in all simulations. This deduction is in accordance with the similar studies in Literature [58, 59]. Boundary conditions are defined as velocity inlet and pressure outlet. Inlet boundary conditions are syngas entrance velocity, temperature and mole fraction of species. Moreover, for cooling fluid fed to system in counter-current route, inlet temperature is defined as the equal with syngas inlet temperature for all cases. Outlet boundary condition defined exit gauge pressure. The boundaries on wall surfaces are taken as no-slip condition. Homogeneous reactions which take place on gas phase over 1000 K are neglected [60], owing to the fact that the reaction medium does not reach the limit value. Therefore, only heterogeneously formed reactions, which means occur in porous catalytic layers, are taken into account.

The properties of fluid mixture and catalyst layer, such as molecular weight, Knudsen and binary diffusivity, thermal conductivity and heat capacity, viscosity, density, are complied from the literature [11, 16, 45]. Temperature dependent correlations are calculated at constant temperatures, due to the fact that divergence of reaction temperature remains below $\sim$20 K for each simulation when it is compared with corresponding initial values. This assumption can be advocated with unchanged results of methane steam reforming conducted over 850 K in a microchannel reactor [61]. Textural and physical properties of the catalysts are adapted from the literature; tortuosity and porosity of the Cu–ZnO/Al_2O_3 and γ–Al_2O_3 catalysts are taken as 1.64 and 0.61,

and 1.72 and 0.58, respectively [17]. It is assumed that both catalysts have the same thermal conductivity of 24.2 W m^{-1} K^{-1} and pores in both catalysts have cylindrical cross–sections with average diameters of 1.14×10^{-8} m (Cu–ZnO/Al_2O_3) and 6.4×10^{-9} m (γ–Al_2O_3) [17]. As mentioned in Section 3.1, the mixed configuration refers the physical mixture of Cu–ZnO/Al_2O_3 and γ–Al_2O_3 catalysts with equal mass ratio (1:1), on the other hand, the opposing bed indicates those catalyst are separately coated inside of the channel walls with equal amounts.

The set of nonlinear partial differential equations which forms momentum, heat and mass transfer equations in 2D geometry, namely x and y direction, are solved under ANSYS Fluent (version:19.2) by means of finite volume technique which is the most well-known tool used in solution of Computational Fluid Dynamics (CFD) problems. Reactor model geometries are prepared and meshed under Gambit 2.3.16 software. Number of total cells for the mixed configuration (Fig. 3.1) 4.05×10^5. The solid wall, the catalyst block, half of reaction and cooling channel is discretized by 2.6×10^5,1.3×10^4, 2.6×10^4 and 3.9×10^4 cells, respectively. On the other hand, solid walls, two half cooling channels, one reaction channel, Cu–ZnO/Al_2O_3 and γ–Al_2O_3 catalyst layers composed of the opposing bed unit cell (Fig. 3.2) is meshed by 1.16×10^6, 1.8×10^5, 1.3×10^5, 2×10^4 and 4×10^4 nodes. Mesh independency is checked for both configurations and difference between all simulation runs are under 1%. Therefore, the proposed meshing pattern is used to produce results reported here.

The kinetic model (Equations 2.1-2.3) together with the correlations used to estimate mixture properties are implemented to the numerical solution in the form of user–defined functions, the set of codes hooked to ANSYS structure. Numerical execution is performed on a HP Z800 workstation equipped with 48 GB of memory. Responses of the reactor configurations against changes in the operating parameters are reported in terms of spatial temperature and reaction rate profiles obtained at the catalyst–fluid interface(s) of the reaction channels, CO and CO_2 conversions, and yields of H_2O and DME. Conversion is defined as the ratio of the molar flow rate of the pertinent species (CO or CO_2) converted to the corresponding species inlet molar flow rate, while the yield of species i is defined as the ratio of molar flow rate of species i in

the product mixture to that of CO at the inlet. Molar flow rate of species i (mol s^{-1}) is obtained from the product of channel cross–sectional area (m^2), surface–averaged linear velocity (m s^{-1}) and surface–averaged concentration of species i (mol m^{-3}).

3.3.1. Working Equations

2D Navier-Stokes equations composed of partial differential equations of mass, heat and momentum conservation are used to simulate the catalytic microchannel reactor, as illustrated in Figures 3.1 and 3.2. Velocity, species concentration and temperature distribution in the reaction channel is obtained by solving those equations. Continuity equation:

$$\nabla.(\rho_m \vec{\mathbf{v}}) = 0 \tag{3.10}$$

Momentum conservation equation (FP): Conservation of momentum is calculated for both reaction and cooling channel flow as follows:

$$\nabla.(\rho_m \vec{\mathbf{v}}\vec{\mathbf{v}}) = \nabla p + \nabla.[\mu_m(\nabla\vec{\mathbf{v}} + (\nabla\vec{\mathbf{v}})^\gamma - \frac{2}{3}(\nabla.\vec{\mathbf{v}})\mathbf{I})] \tag{3.11}$$

Momentum conservation equation (CWP): Conservation of momentum is calculated for porous catalyst layer using the derivative form of 2D cartesian coordinate system of following equation set.

$$\nabla.(\rho_m \vec{\mathbf{v}}\vec{\mathbf{v}}) = \vec{\mathbf{F}} - \nabla p + \nabla.[\mu_m(\nabla\vec{\mathbf{v}} + (\nabla\vec{\mathbf{v}})^\gamma - \frac{2}{3}(\nabla.\vec{\mathbf{v}})\mathbf{I})] \tag{3.12}$$

If feed gas is incompressible, the following term can be neglected:

$$(\nabla.\vec{\mathbf{v}}) = 0 \tag{3.13}$$

$$\vec{\mathbf{F}} = -(\frac{\mu_m}{\alpha}\vec{\mathbf{v}} + \frac{C_2}{2}\rho_m|\vec{\mathbf{v}}|\vec{\mathbf{v}}) \tag{3.14}$$

$$\alpha = \frac{d_p^2}{150}\frac{\epsilon_{cat}^3}{(1-\epsilon_{cat})^2} \tag{3.15}$$

$$C_2 = \frac{3.5}{d_P}\frac{(1-\epsilon_{cat})}{\epsilon_{cat}^3} \tag{3.16}$$

Species mass transport equation (FP): Species mass conservation in fluid phase, where is no reaction, is computed using following equation set.

$$\nabla.(\mu_m\vec{\mathbf{v}}Y_i) = -\nabla.\vec{J}_i \tag{3.17}$$

$$\vec{J}_i = -\rho_m D_{i,m}\nabla Y_i \tag{3.18}$$

Species mass transport equation (CWP-Cu–ZnO/Al_2O_3): Based on species conversion, mass transport which take place over synthesis catalyst can be described by following equation sets.

$$\nabla.(\mu_m\vec{\mathbf{v}}Y_i) = -\nabla.\vec{J}_i + M_i R_i \tag{3.19}$$

$$\vec{J}_i = -\rho_m D_{eff,i,m}\nabla Y_i \tag{3.20}$$

CO balance:

$$R_{CO} = -r_{MS1} \tag{3.21}$$

H_2 balance:

$$R_{H_2} = -2r_{MS1} - 3r_{MS2} \tag{3.22}$$

CH_3OH balance:

$$R_{CH_3OH} = r_{MS1} + r_{MS2} \tag{3.23}$$

CO_2 balance:

$$R_{CO_2} = -r_{MS2} \tag{3.24}$$

H_2O balance:

$$R_{H_2O} = r_{MS2} \tag{3.25}$$

Species mass transport equation (CWP-γ–Al_2O_3): Based on species conversion, mass transport which take place over dehydration catalyst can be described by following equations.

CH_3OCH_3 (DME) balance:

$$R_{CH_3OCH_3} = r_{MD} \tag{3.26}$$

CH_3OH balance:

$$R_{CH_3OH} = -2r_{MD} \tag{3.27}$$

H_2O balance:

$$R_{H_2O} = r_{MD} \tag{3.28}$$

Energy equation (FP): Energy conservation of gas mixture along the fluid channel, which reaction does not exist, can be calculated using thermal conductivity as a function of temperature.

$$\nabla.(c_{p,m}\vec{\mathbf{v}}T) = \nabla.(k_m \nabla T) \tag{3.29}$$

Energy equation (CWP): Energy conservation in the porous catalyst layers can be described taking into account heat generation resulted from exothermic reactions, which takes place both Cu based and aluminum catalysts layers.

$$\nabla.(c_{p,m}\vec{\mathbf{v}}T) = \nabla.(k_{eff,m} \nabla T) + \sum_{rxn}(-\Delta H_{rxn})(r_{rxn}) \tag{3.30}$$

Energy equation (SW): No energy is supplied by solid walls.

$$\nabla.(k_w \nabla T) = 0 \tag{3.31}$$

4. RESULTS AND DISCUSSION

Validation of the proposed opposing bed model with its kinetics, influences of inlet temperature, inlet pressure, inlet molar ratio of H_2/CO and H_2/ CO_2 on reactor performance are displayed in Figure 4.1. Owing to the design considerations explained in Chapter 3, the mixed and opposing bed configurations are designed at different reactor length. In order to make an accurate comparison between these two different shapes, axial length of channel is reported as dimensionless. Moreover, to prevent any visual complication on graphs just the highest (508 K) and lowest (493 K) inlet temperature values are reported when it comes to temperature and reaction rates distribution along the channel. Temperature chart of the opposing bed is received over Cu–ZnO/Al_2O_3 and γ–Al_2O_3 catalysts, due to different occurrence locations of methanol synthesis (Reactions 2.1 & 2.2) and dehydration reactions (2.3).

4.1. Model Verification

Reactor unit models are verified with the experimental data adapted from the literature [3]. CO_2 containing sygas with 50 bar pressure is fed to the microreactor at the inlet temperatures of 483, 503 and 508 K and different space velocities of 4.5×10^3 and 15×10^3 Nml $gcat^{-1}$ h^{-1} in the experimental work [3]. Verification of the proposed mathematical model for the mixed bed catalyst configuration is done by another previous study [8]. Model results differentiate with the range of 3-14% between experimental outcomes, both of which are runned at the same inlet and operating conditions [8].

The opposing configuration reactor model is also validated by the experimental data adapted from the same study which confirms the mixed bed model [3]. As demonstrated in Fig. 4.1, predicted syngas (i.e. CO and H_2) conversion is a good agreement with the experimental outcomes.

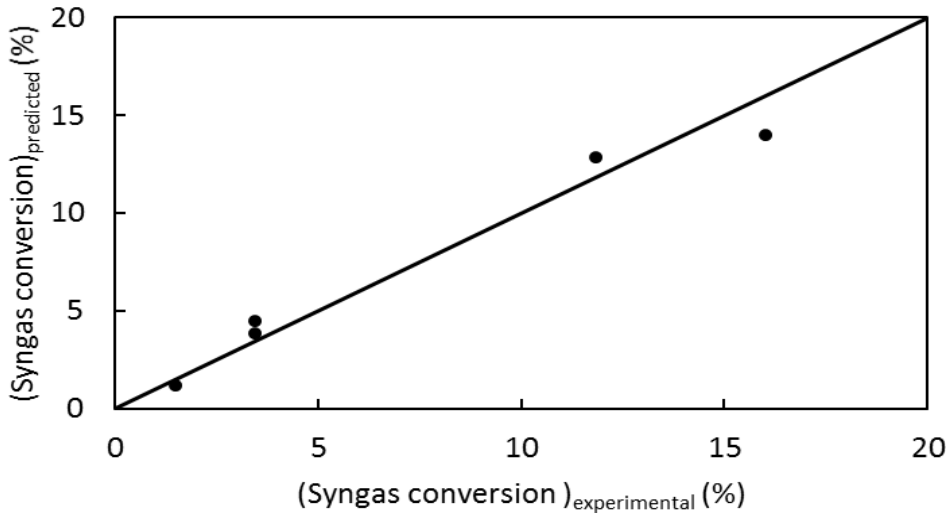

Figure 4.1. The opposing bed model validation by comparing experimental data adapted from [3].

RWGS reaction is implicitly taken into account of the kinetic model equations (Eqs. 2.1- 2.3) and it can be obtained by deducting Reaction 2.2 from 2.1. According to literature, RWGS instantly becomes equilibrium as soon as reaction starts at the studied catalysts and operating conditions [53]. This argument is proved by replacing Reaction 2.2 with RWGS, which means Reaction 2.4 is added to the kinetic model network. A one-dimensional (1D) pseudo homogeneous, steady-state model is constructed to check the presence of RWGS in the used reaction equation models (Eqs. 2.1-2.3). Coupled reaction equilibrium of the kinetics, namely Equations 2.1 and 2.3 is solved by a non-linear algebraic equation solver simultaneously integrated with an ODE solver computed CO hydrogenation and methanol dehydration reaction rates. Extended explanation regarding working and constructing principles of this calculation technique can be found elsewhere [62, 63]. The outcomes are displayed as the difference between hotspot and the syngas initial temperature in Table 4.1. ΔT_1 refers the temperature difference on the elimination of CO_2 hydrogenation from reaction network and coupled Equations 2.1 and 2.3 with RWGS while ΔT_2 shows the temperature divergence created by working kinetic model.

Table 4.1. Temperature divergence between inlet and the hot-spot value according to different cases on the basis of RWGS presence proof.

T_{in}(K)	ΔT_1	ΔT_2
493	3.4	3.8
498	5.1	5.8
503	8.0	9.4
508	13.6	17.1

Table 4.2. DME yield or molar flow rate according to operating conditions (the opposing bed).

Operating condition	Value	DME yield (%) or molar flow rate (x10^{-8} mol s^{-1})
Temperature (K)	493, 498, 503, **508**	1.66, 2.08, 2.6, 3.15
Pressure (bar)	20, 30, **50**, 60	2.65, 2.89, 3.15, 3.2
H_2/CO	**2.5**, 3.5, 4	1.51, 1.49, 1.47
H_2/CO_2	5, 7.5, **10**, 12	2.85, 3.05, 3.15, 3.18

Table 4.3. DME yield or molar flow rate according to operating conditions (the mixed bed).

Operating condition	Value	DME yield (%) or molar flow rate (x10^{-8} mol s^{-1})
Temperature (K)	493, 498, 503, **508**	1.54, 1.91, 2.34, 2.82
Pressure (bar)	20, 30, 40, **50**, 60	2.34, 2.55, 2.67, 2.82, 2.87
H_2/CO	**2.5**, 3.5, 4	1.39, 1.35, 1.33
H_2/CO_2	5, 7.5, **10**, 12	2.62, 2.77, 2.82, 2.82

4.2. Influence of Feed Temperature

Inlet temperature influence on the reaction temperature, reaction rates, CO conversion, CO_2 conversion, yields of steam and methanol are obtained by changing feed temperature from 493 to 508 K with 5 K increments while other parameters are constant at their default values, presented in Figure 4.2. The system temperature rapidly increases to the peak point near the entrance of the channel, and then, slowly decreases along the reaction channel due to external cooling effect (Figure 4.2a).The maximum temperature divergence is computed below 8 K, on the other hand, a conventional micro packed bed reactor runned at the same operating conditions approximately demonstrates hot spot formation as 40 K [2]. This evidence strongly indicates heat transfer capability of microchannel reactors. Two different hot-spot formations which belong to methanol synthesis and dehydration reactions are separately obtained due to the fact that Cu–ZnO/Al_2O_3 and γ–Al_2O_3 catalyst are wash-coated to opposing sides of the reaction channel with facing each other and temperature profiles are received from those layers. It can be clearly seen that, as inlet feed temperature rises, the maximum value of reaction medium temperature increases due to reaction rates are thermodynamically favoured with rising inlet temperature. Mixed configuration demonstrates higher hotspot formation than the opposing bed, due to simultaneous reaction occurence over the same catalyst surface. On the other hand, in the opposing bed, temperature rise is somewhat stiff over Cu–ZnO/Al_2O_3 catalyst due to exothermicity of reactions taking place on. Temperature control can be easier on the opposing configuration owing to homogeneous heat distribution.

The main reason of the rapid rise in the gas mixture temperature at the channel inlet is regarding the high rate of methanol synthesis reactions which occur over Cu–ZnO/Al_2O_3 catalyst (Figure 4.2b). Due to high exothermicity, the rates of Reactions 2.1 and 2.2 decelerate or even turn back in higher temperature values, CO_2 hydrogenation goes down below zero with a faster rate on the mixed bed (Figure 4.2c).

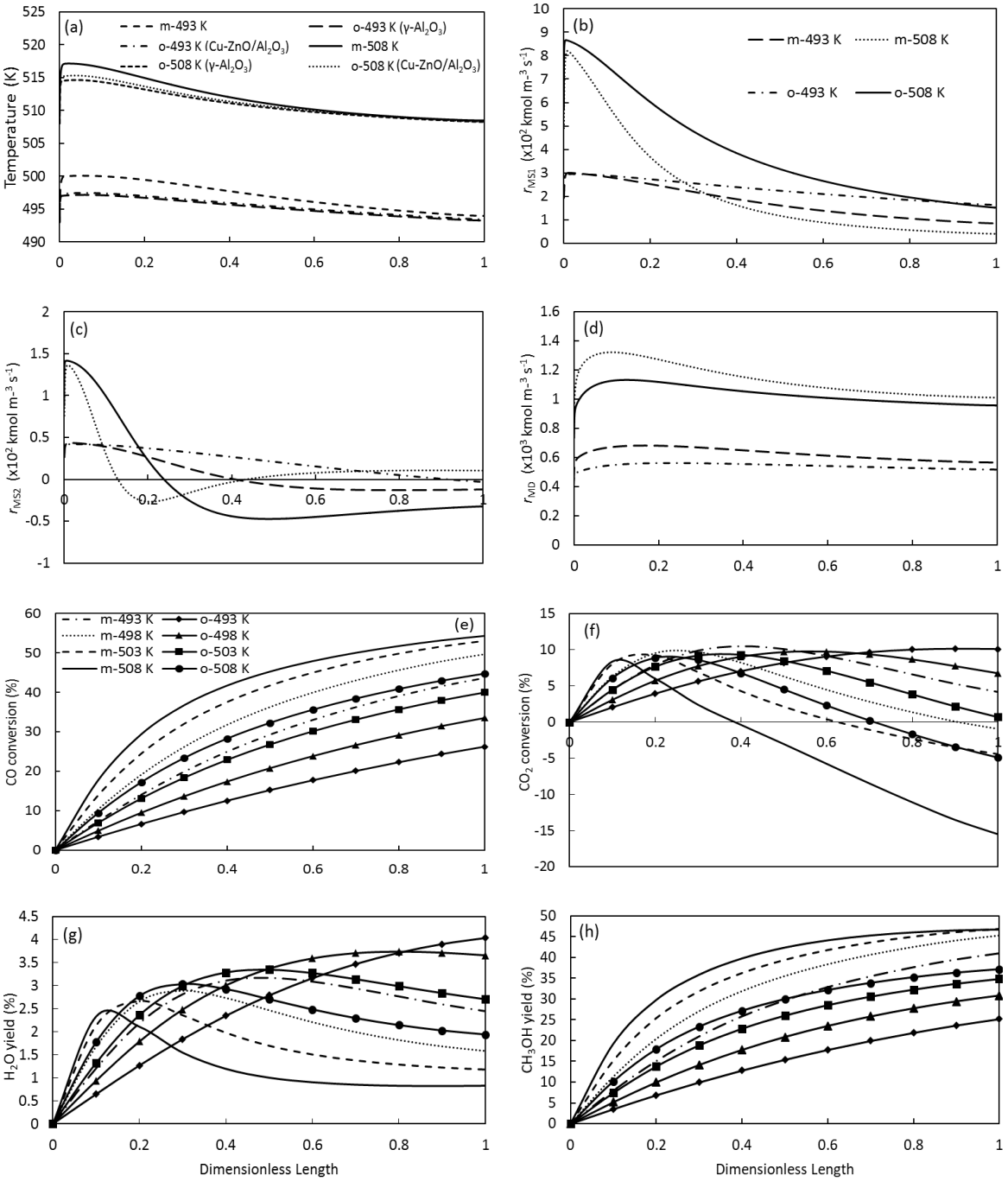

Figure 4.2. Change of temperature (a), reaction rates of CO and CO_2 hydrogenation (b and c), reaction rate of methanol dehydration (d), CO conversion (e), CO_2 conversion (f), steam and methanol yield (g and h) along the reaction channel at different feed stream temperatures.

The rate of DME synthesis reaction, which is one order of magnitude lower than the methanol synthesis reactions, at different feed temperatures are reported in Figure 4.2d. Due to excess amount of methanol in the reaction medium, the rate of DME synthesis reaction is accelerated up to one-fifth of the channel length, and then, the trend of DME synthesis rate continues in accordance with the corresponding temperature. Moreover, in the mixed configuration, reaction rate of methanol dehydration is higher owing to the same reason.

The effect of temperature on spatial evolution of CO and CO_2 conversion is introduced in Figures 4.2e and f, respectively. Increasing initial temperature of feed promotes CO consumption which is also in a good agreement with temperature profiles for both configurations. The mixed bed gives the best performance in terms of syngas conversion due to temperature gap between the opposing counterpart. However, the same situation is not valid for the mixed bed when it comes to CO_2 conversion. In all cases, the opposing coated bed gives the best performance with respect to the mixed configuration in terms of greenhouse gas (CO_2) consumption. Reaction rate of CO_2 hydrogenation justifies positive conversion trend particularly in lower inlet temperature (i.e. 493 K). Since produced methanol, as a result of syngas conversion accelerated by higher inlet temperature, suppresses CO_2 hydrogenation.

Steam is a product of Reactions 2.2 and 2.3. It leads to catalyst deactivation and decreases the reactor performance [30]. Increasing steam content in reaction channel shifts the rate to the reactant side, so yield of steam rapidly increases and then decelerates CO_2 conversion by suppressing Reaction 2.2. The opposing bed shows resistance to excess steam rather than the mixed bed. Methanol is mostly provided by Reactions 2.1 which dictates the reaction system with the highest rate in all configurations (Figure 4.2 h). The mixed bed demonstrates higher methanol yield which is also in accordance with CO conversion profile. DME yield change with increasing temperature is presented in Tables 4.2 and 4.3. DME formation is favoured under risen temperature on both configurations. In particular, the opposing bed clearly shows better performance than the mixed bed due to lower hot-spot formation.

4.3. Influence of Feed Pressure

Inlet pressure effect on the reaction channel temperature, reaction rate of CO and CO_2 hydrogenation, CO and CO_2 conversions, yields of steam and methanol is reported by changing feed pressure as 20,30 and 60 bar, presented in Figure 4.3. To prevent any visual complication on graphs just the highest (60 bar) and lowest (20 bar) inlet syngas feed pressure influence on the evolution of reaction channel temperature and on the rates of reactions are reported. Increasing feed pressure promotes the reaction channel temperatures, as presented in Figure 4.3a. Temperature of the channel rises at the inlet and then is decreased for the rest of the channel due to enabled air cooling to the system. The most important reason of temperature peak in the channel inlet is exothermic reaction activity of syngas conversion to methanol reactions, illustrated in Figs. 4.3b and c. Since, a gas-phase reaction shifts to the side with a fewer number of molecules under high pressures as implied by Le Chatelier's principle of thermodynamic of the gases [64]. Reaction rates significantly rise with increasing feed pressure at the value of 60 bar. This promotion, however, declines forward of the channel owing to the stronger thermodynamic resistance forced by pressure-induced exothermic heat release which absolutely much more in the mixed configuration, therefore, especially, the rate of 2.1 sharply decreases.

Conversion evolution of CO with increasing pressure is reported in Figures 4.3e. CO conversion increases from ∼25% to ∼60% on the mixed bed and rises from ∼21% to ∼49% on the opposing bed, a a result of changing pressure in a range of 20 and 60 bar (Figure 4.3e). Better performance of the mixed bed in terms of syngas conversion can be attributed to sharp temperature increase in the reaction channel. Positive effect of increasing pressure on syngas conversion can be explained by Le Chatelier's thermodynamics of gases principle [64]. The importance of this effect on the opposing bed is observed at the lowest pressure particularly, for instance rising pressure from 20 bar to 30 bar elevates CO conversion 45%, whereas, changing from 50 bar to 60 bar improves conversion 11%.

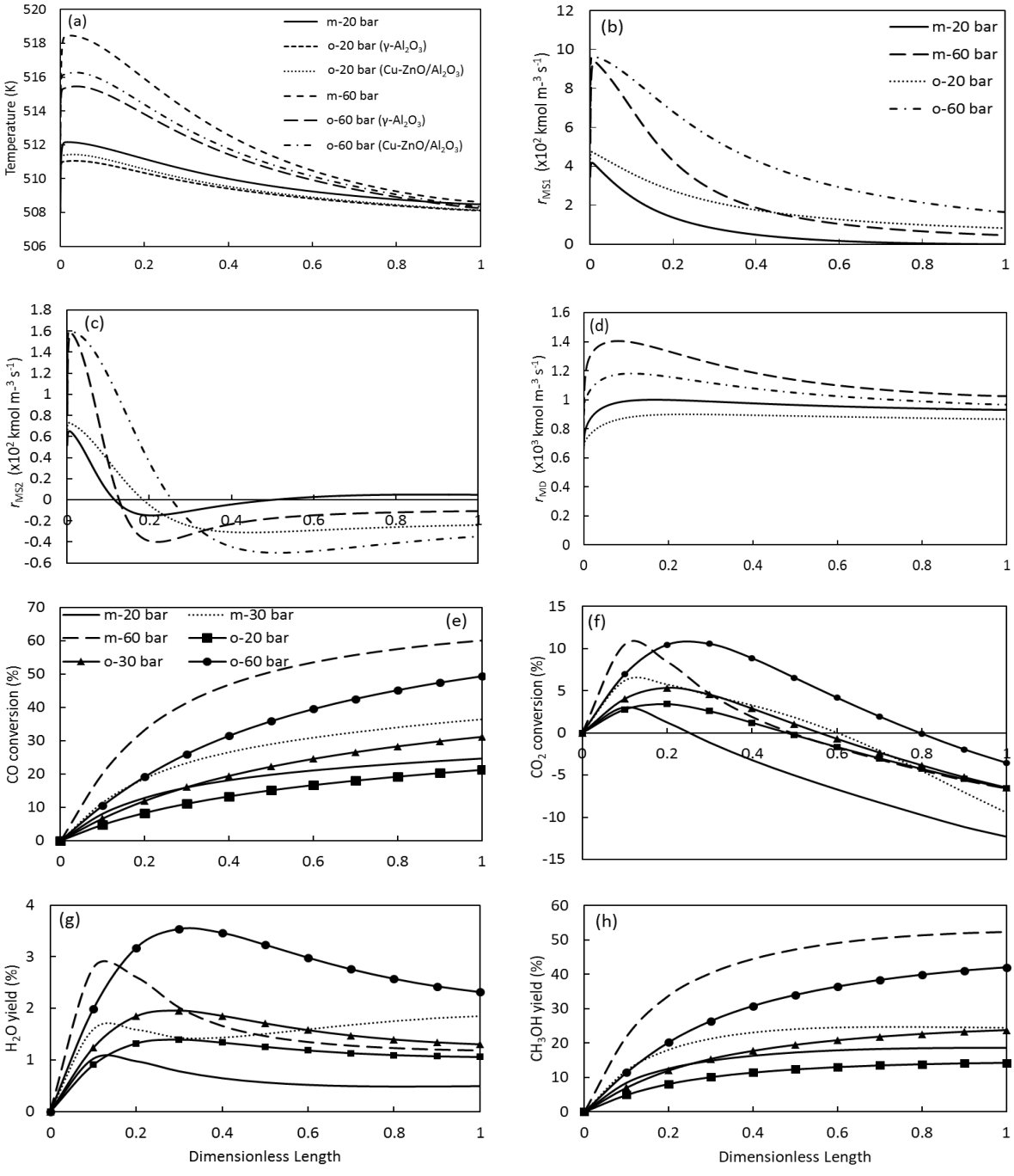

Figure 4.3. Change of temperature (a), reaction rates of CO and CO_2 hydrogenation (b and c), reaction rate of methanol dehydration (d), CO conversion (e), CO_2 conversion (f), steam and methanol yield (g and h) along the reaction channel at different feed stream pressures.

CO_2 conversion is elevated on the mixed bed up to maximum value of 10.5% (at 508 K) before one-fifth of the channel, while the peak conversion point on the opposing configuration is observed with the same value at the two-third of the length of the channel. This finding is related to the yield of steam and dehydration rate curves. Steam production rises in the first half of the channel, and then, decreases due to the excess amount of methanol which suppresses Reaction 2.2 for both configurations. The highest steam yield with the value of 3.5% is observed on the opposing coated bed (at 60 bar), whereas, the peak point on the mixed bed is 2.8%. After the maximum value, steam yields and CO_2 conversion profiles diminishes along the channel due to negative thermodynamic impact of continuously increasing methanol formation. Overall, the opposing bed shows a successful performance in increasing pressures in terms of converting the greenhouse gas. Therefore, separately washcoated synthesis and dehydration catalysts facing opposite to each other is considered as a promising candidate from an environmental point of view.

Methanol yield profile is presented in Figure 4.3f. Methanol yields are in accordance with those of CO conversion, it is strong evidence of the profound influence of CO hydrogenation on methanol synthesis (Figure 4.3h). Besides Reaction 2.1, CO_2 hydrogenation has a role on methanol formation. Figure 4.2 d shows the axial distribution of Reaction 2.3. Methanol dehydration is notably promoted by methanol feedstock reactions (Reactions 2.1 and 2.2). Moreover, the mixed bed presents better performance with elevated pressures in terms of DME synthesis reaction (Reaction 2.3) accelerated by excess methanol in the reaction medium.

DME formation remain unresponsive to pressure elevation after 50 bar due to the fact that methanol dehydration reaction is in stoichiometric balance. On the opposing bed, DME yield changes between 2.65% and 2.89% (Table 4.2), whereas, on the mixed bed, this value is calculated as 2.34-2.55%, both of which are computed the pressure range of 20-30 bar. On the other hand, altering pressure between 50-60 bar rises DME yield from 3.15% to 3.2% and between 2.82-2.87% on the opposing and the mixed bed, respectively.

4.4. Influence of H_2/CO Feed ratio

Inlet molar H_2/CO ratio effect on the reaction channel temperature, reaction rate of CO and CO_2 hydrogenation, CO conversion, CO_2 conversion, yields of steam and methanol are reported by changing H_2/CO feed ratios as 2.5, 3.5 and 4, as presented in Figure 4.4. The ratio is determined by keeping the molar flow rate of H_2 and gas mixture constant, while the molar flow rate of CO is changing by means of controlling N_2 (inert) flow rate. Other reactor parameters are kept constant at their operating values, while investigating the effect of molar flow rate of CO in the feed stream.

The system temperature quickly increases and reaches the maximum point at the entrance and then decreases along the reaction channel due to the integrated cooling stream (Figure 4.4a). On both configurations, commonly, as H_2/CO ratios decrease, temperature profiles attain peak points and decrease with faster rates. This behavior can be attributed to high inert content in the feed stream.

The rates of Reaction 2.1 and 2.2 plotted in Figures4.4b and c give an explanation regarding the influence of feed ratio. The rate of CO hydrogenation reaction achieves higher values with decreasing ratios which indicate increasing CO content in the feed stream. This behaviour is in accordance with the temperature evolution curves (Figure 4.4a). On the mixed bed, due to faster decline of CO-to-methanol synthesis rate, CO conversion achieves higher values. CO_2 hydrogenation rate shows higher improvement under CO-lean conditions due to excess methanol produced from CO hydrogenation hampers CO_2-to-methanol synthesis rate (Figure 4.4c).

The rate of Reaction 2.3 is plotted at different H_2/CO ratios in Figure 4.4d. DME synthesis reaction rate order is one-tenth of CO-to-methanol synthesis rate, which dominates the temperature profile, the influence of heat released by Reaction 2.3 on the system temperature remains insignificant on account of its impotent dehydration rate and follows the trend of temperature distribution.

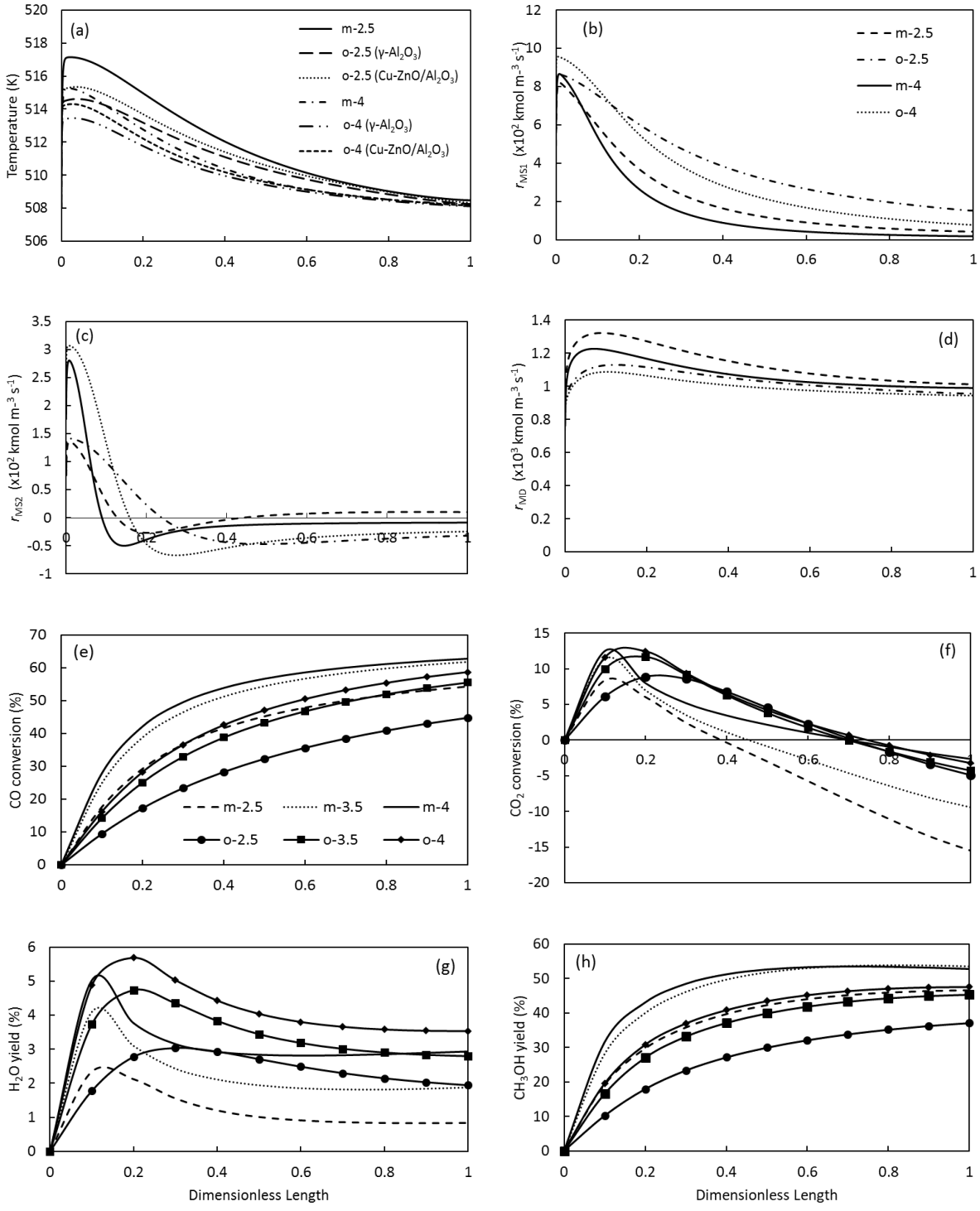

Figure 4.4. Change of temperature (a), reaction rates of CO and CO_2 hydrogenation (b and c), reaction rate of methanol dehydration (d), CO conversion (e), CO_2 conversion (f), steam and methanol yield (g and h) along the reaction channel at different inlet molar H_2/CO ratio.

In spite of decreasing CO content in the feed stream, CO-lean conditions show higher CO conversions as a result of its calculation method, explained in elsewhere [8]. The molar flow rates of consumed CO decreases as 1.95×10^{-7}, 1.6×10^{-7}, 1.42×10^{-7} mol s^{-1} on the mixed bed, while decreases on the opposing bed in the order of 1.61×10^{-7}, 1.44×10^{-7}, 1.33×10^{-7} mol s^{-1} at the ratios of 2.5, 3.5 and 4, respectively. This finding is also in accordance with the axial temperature distribution profiles for both configurations at the corresponding values. Mixing methanol synthesis and dehydration catalysts provides higher CO consumption due to instant methanol dehydration.

CO_2 conversion is illustrated as a function of channel length in Figure 4.4f. It is obvious that the mixed configuration does not promote CO_2 hydrogenation other than the ratio of 4 which also shows a good agreement with steam yield. Released heat by CO hydrogenation dampers CO_2 conversion. Changing CO ratio on the opposing bed remain ineffective as of 30% of the channel. The maximum value of CO_2 conversion on both configurations are observed as 13% under CO-lean conditions.

Yields of steam and methanol dependent on inlet molar H_2/CO ratio are presented in Figures 4.4g and h. Yield calculations are made on the basis of CO molar flow rate, therefore, taking into account the exit molar flow rates of steam and methanol is considered as a more reliable way owing to the ratio change of CO in the inlet stream. The quantity of discharged steam is computed as 3.39×10^{-9}, 5.28×10^{-9} and 7.06×10^{-9} mol s^{-1} on the mixed bed, while it is calculated as 7.4×10^{-9}, 7.66×10^{-9} and 8.42×10^{-9} mol s^{-1} on the opposing bed, both of which are at H_2/CO ratios of 2.5, 3.5 and 4, respectively. It is obvious that contribution of Reaction 2.3 to H_2O formation remains negligible compared with Reaction 2.2. Presence of RWGS reaction, which is a combination of Reaction 2.1 and 2.2, is proved due to accelerated steam production under CO-lean operating conditions. The amount of methanol at the reactor outlet is reported as 1.74×10^{-7}, 1.45×10^{-7} and 1.26×10^{-7} mol s^{-1} on the mixed bed, while it is computed as 1.4×10^{-7}, 1.24×10^{-7} and 1.14×10^{-7} mol s^{-1} on the opposing bed, both of which at H_2/CO ratios of 2.5, 3.5 and 4, respectively. This patter is completely different from reported methanol yield distribution presented in Figure 4.4h. The highest methanol amount is observed on the mixed bed catalyst, as expected, owing

to the highest CO consumption. Produced amount of methanol by Reaction 2.2 can be found by deducting the amount of consumed CO, also has the same value with methanol contributed by Reaction 2.1, from the exit methanol amount. The results are calculated on the mixed bed as -2.12×10^{-8}, -1.48×10^{-8} and -1.6×10^{-8}, while on the opposing bed, calculated as -2.11×10^{-8}, -2×10^{-8} and -1.9×10^{-8} at the ratios of 2.5, 3.5 and 4, respectively. Although methanol flow rates are negative, which means methanol consumption, this can be posed as a proof of negative CO_2 conversion as of 80% of the channel. Methanol is consumed by reverse CO_2 hydrogenation reaction due to in-situ H_2O formation.

The highest amount of produced DME is obtained as 8.42×10^{-9} and 1.51×10^{-8} mol s^{-1} on the mixed bed and opposing bed, respectively, at the H_2/CO ratio of 2.5. In the frame of this result, the opposing configuration can be offered as the best option in terms of efficient DME production at CO-rich condition.

4.5. Influence of H_2/CO_2 Feed ratio

Inlet molar H_2/CO_2 ratio effect on the reaction channel temperature, reaction rate of CO and CO_2 hydrogenation, CO and CO_2 conversions, yields of steam and methanol are reported by changing H_2/CO feed ratios as 5, 7.5, 10 and 12, as presented in Figure 4.5. Studying ratios are regulated by changing inert gas flow rate while keeping the H_2 amount stable in the total feed stream, so the same strategy explained in Section 4.4 is implemented.

Reaction channel temperature rises on reducing CO_2 content in the syngas feed stream (Figure 4.5a). Temperature change with increasing ratio is calculated as 5 and 9 K on the mixed bed, whereas the difference on the opposing bed is computed as 3 and 7 K at the ratios of 5 and 12, respectively. CO_2-rich conditions suppress CO hydrogenation, which is the most exothermic reaction among the kinetic model reactions, thus temperature of the reaction channel decreases from the value of hot-spot formation, where occurs on the channel entrance. Dominance of mildly exothermic synthesis reactions provide higher temperatures at the Cu–ZnO/Al_2O_3–fluid interface.

On the mixed bed, temperature gap is higher due to be involved of dehydration reaction (Figure 4.5a).

The axial temperature distribution is in accordance with reaction rates of CO hydrogenation, as presented in Figure 4.5b. Under CO_2-lean conditions, CO hydrogenation is promoted due to lack of produced methanol in the reaction medium by CO_2 hydrogenation (Figure 4.5b). Similarly, increasing CO_2 content in the system by adjusting H_2/CO_2 as 5 diminishes Reaction 2.1 and also decreases the channel temperature.

Alteration of CO_2 hydrogenation reaction rate is reported in Figure 4.5c with the inlet H_2/CO_2 on increasing order as 5 and 12 on both the mixed and the opposing configurations. Reaction trend peaks at the channel inlet under CO_2-lean conditions due to released heat from CO hydrogenation, which dominates the system particularly under lack of CO_2 in the feed stream. On the other hand, increasing CO_2 content in the feed syngas by adjusting the ratio of 5 remains the reaction curve over positive side and hinders reverse route of CO_2 hydrogenation both thermodynamically and kinetically. This behavior is particularly observed on the opposing bed.

Diminished CO_2 level leads to slight gab between ratios in terms of methanol dehydration reaction rates, particularly on the mixed bed, nearly one-fifth of the channel length (Figure 4.5d). However, there is no sharp difference between ratios of 10 and 12, therefore, ratio of 10 can be selected for both optimizing reaction performance and reducing green house gas.

CO conversion decreases with increasing molar inlet H_2/CO_2 ratio, as presented in Figure 4.5e. On the both catalyst configurations, it is clearly observed that CO conversion remains unresponsive beneath the ratio of 10. CO_2 conversion change along the channel is reported in Figure 4.5f. However, due to altering CO_2 amount in the feed stream, the differences between inlet and outlet CO_2 flow rates are calculated as 1.3×10^{-8}, 5.28×10^{-9}, -4.2×10^{-9} and -6.2×10^{-9} mol s^{-1} on the opposing bed, whereas, on the mixed bed, it is calculated as 4.1×10^{-9}, -6.7×10^{-9}, -1.6×10^{-8} and -3.1×10^{-8} mol s^{-1}

at the molar inlet H_2/CO_2 ratios of 5, 7.5, 10 and 12, respectively. The reason of those decreasing order can be explained by rate of reaction 2.2 which passes the negative side. The opposing configuration shows the most effective performance under CO_2-rich condition.

Steam formation is boosted due to elevated CO_2 content in the feed stream, illustrated in Figure 4.5g. The trend of steam yield is also in accordance with CO_2 consumption values. The positive correlations between steam yield and CO_2 consumption values pose a proof of negligible contribution of methanol dehydration reaction to H_2O formation. Steam formation on opposing bed does not turned back under CO_2-rich condition owing to kinetically and thermodynamically favoured Reaction 2.2 at slightly lower temperature condition.

Reported methanol yield results, where in Figure 4.5h, give a comprehensive opinion regarding the role of CO hydrogenation on methanol synthesis. It is concluded that increasing CO_2 content in the feed stream has a negative impact on methanol production. The mixed bed configuration shows more efficient performance on methanol synthesis due to attaining higher CO conversion compared to the opposing bed.

DME yield results in terms of percentage are reported in Tables 4.2 and 4.3, respectively. DME formation over the opposing bed is much more efficient than the mixed bed. Adjusting the ratio between 5-7.5 rises DME yield in the range of 2.85-3.05% and 2.62-2.77% on the opposing and the mixed bed, respectively. After the ratio of 10, DME formation remains unresponsive.

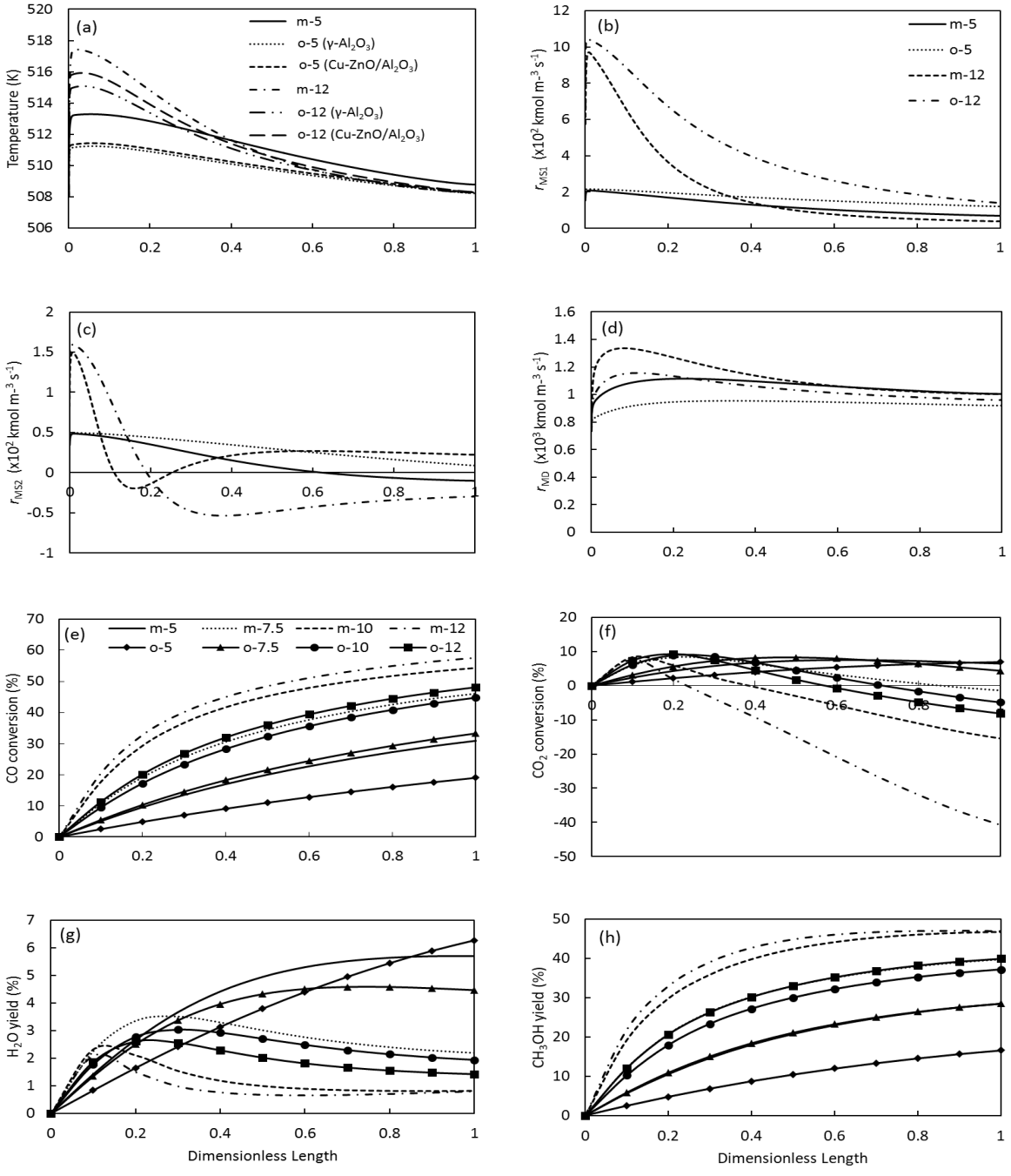

Figure 4.5. Change of temperature (a), reaction rates of CO and CO_2 hydrogenation (b and c), reaction rate of methanol dehydration (d), CO conversion (e), CO_2 conversion (f), steam and methanol yields (g and h) along the reaction channel at different inlet molar H_2/CO_2 ratio.

5. CONCLUSIONS AND RECOMMENDATIONS

5.1. Conclusions

In this study, syngas including CO_2 feedstock is utilized to produce DME in a heat exchange integrated microchannel reactor. Two reactor configurations are compared in terms of methanol synthesis and dehydration catalysts coating structure, namely the mixed and the opposing bed configurations. In the mixed bed, methanol synthesis and dehydration reactions are considered take place on the same catalyst surface which composed as a unique mixing of Cu–ZnO/Al_2O_3 and γ–Al_2O_3 catalysts, the thickness of catalyst layer is calculated as 5×10^{-5} m. On the other hand, in the opposing bed, methanol synthesis (Cu–ZnO/Al_2O_3) and dehydration catalyst (γ–Al_2O_3) are separately coated on the both sides of the reaction channel walls facing opposite to each other, the layer thickness of both synthesis and dehydration catalysts are computed as 2.5×10^{-5} and 5×10^{-5} m, respectively. The solid wall is located between the reaction and cooling channel to remove the released heat from reaction medium to air-cooled channel through conduction heat transfer. Simulation of this process is conducted under ANSYS-Fluent environment by solving two dimensional conservation of mass, energy and momentum equations integrated with reaction transport in the porous catalyst layer by means of finite volume method. Based on the comparison of two reactor configuration, this study can briefly be concluded as follows:

- The hot-spot formation near the entrance of the reaction channel is observed in all cases on both configurations, however, it remains in limited level (below 8 K) due to integrated cooling. In conventional packed bed reactors, the temperature difference is reported as $\sim$40 K for the direct conversion of syngas to DME in literature.
- Direct DME synthesis reaction is mostly controlled by CO hydrogenation, which is the reason of hot-spot formation at the channel inlet. Elevated temperature and pressure have positive impact on DME synthesis reactions, CO conversion is promoted up to 60% and 49% on the mixed bed and the opposing bed, respec-

tively. DME yield is observed as 2.82% on the mixed bed, while it is obtained on the opposing bed as 3.2%.

- Due to increasing rates of CO hydrogenation, in situ accumulation of methanol hampers CO_2 conversions at higher temperatures on the both configurations. Feeding syngas below 498 K to reduce the rate of CO hydrogenation or enriching syngas with CO_2 to obtain $H_2/CO_2 < 7.5$ and promote CO_2 hydrogenation ends up with positive CO_2 conversions up to $\sim$10.5% on the opposing bed.

5.2. Recommendations

The recommendations for inspiring further studies regarding direct DME synthesis can be given as follows:

- Reaction channel can be coated with different amount of synthesis and dehydration catalysts due to lower reaction rate of methanol dehydration reaction.
- Synthesis and dehydration catalysts can be coated to channel wall in a sequential order.
- Different reactor and catalyst geometries, i.e. zig-zag reactor geometry, can be utilized to attain effective heat and mass transfer rates.
- Velocity of coolant air can be increased to prevent temperature peak points and observed isothermal condition effect on the reactor performance.
- A sequential reaction-cooling system can be established by positioning intercoolers betweeen microchannel reactors, connected to each other, to investigate influence of local adiabatic operation on reactor performance.
- Cooling channel pressure can be decreased to reduce operating cost.
- A perm selective membrane can be integrated to catalyst-fluid surface to provide in situ removal of steam.

REFERENCES

1. Park, S. H. and C. S. Lee, "Applicability of dimethyl ether (DME) in a compression ignition engine as an alternative fuel", *Energy Conversion and Management*, Vol. 86, pp. 848 – 863, 2014.

2. Hu, Y., Z. Nie and D. Fang, "Simulation and model design of pipe-shell reactor for the direct synthesis of dimethyl ether from syngas", *Journal of Natural Gas Chemistry*, Vol. 17, pp. 195–200, 2008.

3. Hayer, F., H. Bakhtiary-Davijany, R. Myrstad, A. Holmen, P. Pfeifer and H. J. Venvik, "Modeling and simulatiofn of an integrated micro packed bed reactor-heat exchanger configuration for direct dimethyl ether synthesis", *Topics in Catalysis*, Vol. 54, p. 817, 2011.

4. Jiang, Q., *Direct dimethyl ether synthesis from CO_2/H_2*, Ph.D. Thesis, Université de Strasbourg, 2017.

5. Samimi, F., M. Bayat, D. Karimipourfard, M. Rahimpour and P. Keshavarz, "A novel axial-flow spherical packed-bed membrane reactor for dimethyl ether synthesis: Simulation and optimization", *Journal of Natural Gas Science and Engineering*, Vol. 13, pp. 42 – 51, 2013.

6. Papari, S., M. Kazemeini and M. Fattahi, "Mathematical modeling of a slurry reactor for DME direct synthesis from syngas", *Journal of Natural Gas Chemistry*, Vol. 21, No. 2, pp. 148 – 157, 2012.

7. Iliuta, I., M. C. Iliuta, P. Fongarland and F. Larachi, "Integrated aqueous-phase glycerol reforming to dimethyl ether synthesis—A novel allothermal dual bed membrane reactor concept", *Chemical Engineering Journal*, Vol. 187, pp. 311 – 327, 2012.

8. Ozturk, N. F. and A. K. Avci, "Intensified dimethyl ether production from synthesis gas with CO_2", *Chemical Engineering Journal*, Vol. 370, pp. 885 – 896, 2019.

9. Azizi, Z., M. Rezaeimanesh, T. Tohidian and M. R. Rahimpour, "Dimethyl Ether: A review of Technologies and Production Challenges", *Chemical Engineering and Processing: Process Intensification*, Vol. 82, pp. 150–172, 2014.

10. Goodwin, B. M., *Thermodynamic Properties of Multicomponent Systems, Multicomponent Phase Equilibria and Chemical Equilibria*, American Institute of Chemical Engineers, New York, 1982.

11. Mcbride, B. J., S. Gordon and M. A. Reno, *Coefficients for calculating thermodynamic and transport properties of individual species*, National Aeronautics and Space Administration, 1993.

12. Viswanathan, B. (Editor), *Energy Sources*, Elsevier, Amsterdam, 2017.

13. Martins, J. M., F. Guo and D. A. Swanson, "Chapter 1 - Population: Survival and Growth", *Global Population in Transition*, pp. 1–41, Springer, Cham, 2018.

14. (BP), B. P., *BP Energy Outlook 2019*, 2019, accessed at Dec 2019.

15. Ellabban, O., H. Abu-Rub and F. Blaabjerg, "Renewable energy resources: Current status, future prospects and their enabling technology", *Renewable and Sustainable Energy Reviews*, Vol. 39, pp. 748–764, 2014.

16. Delparish, A. and A. K. Avcı, "Modeling of intensified glycerol steam reforming in a heat- exchange integrated microchannel reactor", *Catalysis Today*, Vol. 299, pp. 328–338, 2018.

17. Peláez, R., P. Marín and S. Ordóñez, "Direct synthesis of dimethyl ether from syngas over mechanical mixtures of $CuO/ZnO/Al_2O_3$ and γ-Al_2O_3: Process optimization and kinetic modelling", *Fuel Processing Technology*, Vol. 168, pp. 40–49,

2017.

18. Vakili, R., E. Pourazadi, P. Setoodeh, R. Eslamloueyan and M. R. Rahimpour, "Direct dimethyl ether (DME) synthesis through a thermally coupled heat exchanger reactor", *Applied Energy*, Vol. 88, pp. 1211–1223, 2011.

19. Erena, J., I. Sierra, A. T. Aguayo, A. Ateka, M. Olazar and J. Bilbao, "Kinetic modelling of dimethyl ether synthesis from (H_2+CO_2) by considering catalyst deactivation", *Chemical Engineering Journal*, Vol. 174, pp. 660–667, 2011.

20. Brand, O., G. K. Fedder, C. Hierold, J. G. Korvink and O. Tabata, *Micro process engineering: fundamentals, devices, fabrication, and applications*, John Wiley & Sons, 2013.

21. Kiwi-Minsker, L. and A. Renken, "Microstructured reactors for catalytic reactions", *Catalysis Today*, Vol. 110, pp. 2–14, 2005.

22. Ehrfeld, W., V. Hessel and H. Löwe, *Microreactors: New Technology for Modern Chemistry*, Wiley WCH, Weinheim, 2016.

23. Hayer, F., H. Bakhtiary-Davijany, R. Myrstad, A. Holmen, P. Pfeifer and H. J. Venvik, "Synthesis of dimethyl ether from syngas in a microchannel reactor—Simulation and experimental study", *Chemical Engineering Journal*, Vol. 167, pp. 610–615, 2011.

24. Kolb, G., "Review: Microstructured reactors for distributed and renewable production of fuels and electrical energy", *Chemical Engineering and Processing*, Vol. 65, pp. 1–44, 2013.

25. Karakaya, M. and A. K. Avci, "Comparison of compact reformer configurations for on-board fuel processing", *International Journal of Hydrogen Energy*, Vol. 35, No. 6, pp. 2305 – 2316, 2010.

26. Bac, S., S. Keskin and A. K. Avcı, "Modeling and simulation of water-gas shift in a heat exchange integrated microchannel converter", *International Journal of Hydrogen Energy*, Vol. 43, pp. 1094–1104, 2018.

27. Saravanan, K., H. Ham, N. Tsubaki and J. W. Bae, "Recent Progress for Direct Synthesis of Dimethyl Ether from Syngas on the Heterogeneous Bifunctional Hybrid Catalysts", *Applied Catalysis B: Environmental*, Vol. 217, pp. 494–522, 2017.

28. Asthana, S., C. Samanta, A. Bhaumik, B. Banerjee, R. K. Voolapalli and B. Saha, "Direct synthesis of dimethyl ether from syngas over Cu-based catalysts: Enhanced selectivity in the presence of MgO", *Journal of Catalysis*, Vol. 334, pp. 89 – 101, 2016.

29. Peláez, R., P. Marín, F. V. Díez and S. Ordóñez, "Direct synthesis of dimethyl ether in multi-tubular fixed-bed reactors: 2D multi-scale modelling and optimum design", *Fuel Processing Technology*, Vol. 174, pp. 149 – 157, 2018.

30. Erena, J., I. Sierra, M. Olazar, A. G. Gayubo and A. T. Aguayo, "Deactivation of a $CuO-ZnO-Al_2O_3/\gamma$–Al_2O_3 catalyst in the synthesis of dimethyl ether", *Industrial and Engineering Chemistry Research*, Vol. 47, pp. 2238–2247, 2008.

31. Kiviranta-Paakkönen, P., L. Struckmann, J. Linnekoski and A. Krause, "Langmuir-Hinshelwood kinetics of the dehydration of methanol catalyzed by cation exchange resin", *Industrial and Engineering Chemistry Research*, Vol. 37, pp. 18–24, 1998.

32. Gates, B. and L. Johanson, "Dehydration of the alcohol in the etherification of isoamylenes with methanol and ethanol", *Industrial and Engineering Chemistry Research*, Vol. 17, pp. 981–983, 1971.

33. Hosseininejad, S., A. Afacan and R. Hayes, "Catalytic and kinetic study of methanol dehydration to dimethyl ether", *Chemical Engineering Research and Design*, Vol. 90, pp. 825–833, 2012.

34. Raoof, F., M. Taghizadeh, A. Eliassi and F. Yaripour, "Effects of temperature and feed composition on catalytic dehydration of methanol to dimethyl ether over γ-alumina", *Fuel*, Vol. 87, pp. 2967–2971, 2008.

35. Rownaghi, A. A., F. Rezaei, M. Stante and J. Hedlund, "Selective dehydration of methanol to dimethyl ether on ZSM-5 nanocrystals", *Applied Catalysis B: Environmental*, Vol. 119-120, pp. 56 – 61, 2012.

36. Zhu, Y., S. Wang, X. Ge, Q. Liu, Z. Luo and K. Cen, "Experimental study of improved two step synthesis for DME production", *Fuel Processing Technology*, Vol. 91, pp. 424–429, 2010.

37. Moradi, G., F. Yaripour and P. Vale-Sheyda, "Catalytic dehydration of methanol to dimethyl ether over mordenite catalysts", *Fuel Process. Technology*, Vol. 91, pp. 461–468, 2009.

38. Hayer, F., H. Bakhtiary-Davijany, R. Myrstad, A. Holmen, P. Pfeifer and H. J. Venvik, "Characteristics of integrated micro packed bed reactor-heat exchanger configurations in the direct synthesis of dimethyl ether", *Chemical Engineering and Processing: Process Intensification*, Vol. 70, pp. 77–85, 2013.

39. Jia, G.-x., H.-b. Ma, Y.-s. Tan and Y.-z. Han, "Effect of Particle Size on the Hybrid Catalyst Activity for Slurry Phase Dimethyl Ether Synthesis", *Industrial and Engineering Chemistry Research*, Vol. 44, No. 7, pp. 2011–2015, 2005.

40. Martínez, A., G. Prieto, A. García-Trenco and E. Peris, *Advanced Catalysts Based on Micro- and Mesoporous Molecular Sieves for the Conversion of Natural Gas to Fuels and Chemicals*, John Wiley & Sons, Ltd, 2010.

41. Cai, M., V. Subramanian, V. V. Sushkevich, V. V. Ordomsky and A. Y. Khodakov, "Effect of Sn additives on the CuZnAl–HZSM-5 hybrid catalysts for the direct DME synthesis from syngas", *Applied Catalysis A: General*, Vol. 502, pp. 370–379, 2015.

42. Abu-Dahrieh, J., D. Rooney, A. Goguet and Y. Saih, "Activity and deactivation studies for direct dimethyl ether synthesis using CuO–ZnO/Al_2O_3 with NH4ZSM-5, HZSM-5 or γ–Al_2O_3", *Chemical Engineering Journal*, Vol. 203, pp. 201 – 211, 2012.

43. Tavan, Y., S. H. Hosseini, M. Ghavipour, M. R. K. Nikou and A. Shariati, "From laboratory experiments to simulation studies of methanol dehydration to produce dimethyl ether—Part I: Reaction kinetic study", *Chemical Engineering and Processing: Process Intensification*, Vol. 73, pp. 144 – 150, 2013.

44. Spivey, J. J., "Rewiev: Dehydration catalysts for the methanol/dimethyl ether reaction", *Chemical Engineering Communications*, Vol. 110, No. 1, pp. 123–142, 1991.

45. Bac, S. and A. K. Avci, "Ethylene oxide synthesis in a wall-coated microchannel reactor with integrated cooling", *Chemical Engineering Journal*, Vol. 377, p. 120104, 2019, iSCRE 25 Special Issue: Bridging Science and Technology.

46. Rebrov, E. V., M. H. J. M. de Croon and J. C. Schouten, "Design of a microstructured reactor with integrated heat-exchanger for optimum performance of a highly exothermic reaction", *Catalysis Today*, Vol. 69, pp. 183–192, 2001.

47. Scott, H. F., *Elements of chemical reaction engineering*, Prentice Hall, 2016.

48. Ogawa, T., N. Inoue, T. Shikada and Y. Ohno, "Direct Dimethyl Ether Synthesis", *Journal of Natural Gas Chemistry*, Vol. 12, No. 4, pp. 219–227, 2003.

49. Iliuta, I., F. Larachi and P. Fongarland, "Dimethyl ether synthesis with in situ H2O removal in fixed-bed membrane reactor: model and simulations", *Industrial and Engineering Chemistry Research*, Vol. 49, pp. 6870–6877, 2010.

50. Stanislao, M. D., A. Malandrino, R. Patrini, C. Pirovano, A. Viva and E. Brunazzi, "DME synthesis via catalytic distillation: Experiments and simulation", V. Pleşu

and P. Şerban Agachi (Editors), *17th European Symposium on Computer Aided Process Engineering*, Vol. 24 of *Computer Aided Chemical Engineering*, pp. 1077 – 1082, Elsevier, 2007.

51. Onsan, Z. I. and A. K. Avcı, "Chapter 14 - Reactor Design for Fuel Processing", D. Shekhawat, J. J. Spivey and D. A. Berry (Editors), *Fuel Cells: Technologies for Fuel Processing*, pp. 451–516, Elsevier Science, Amsterdam, 2011.

52. Uriz, I., G. Arzamendi, E. López, J. Llorca and L. Gandía, "Computational fluid dynamics simulation of ethanol steam reforming in catalytic wall microchannels", *Chemical Engineering Journal*, Vol. 167, pp. 603–609, 2011.

53. Aguayo, A. T., J. Ereña, D. Mier, J. M. Arandes, , M. Olazar and J. Bilbao, "Kinetic modeling of dimethyl ether synthesis in a single step on a CuO-ZnO-Al_2O_3/ γ-Al_2O_3 catalyst", *Industrial and Engineering Chemistry Research*, Vol. 46, 2007.

54. Sun, J. T., I. S. Metcalfe and M. Sahibzada, "Deactivation of Cu/ZnO/Al_2O_3 methanol synthesis catalyst by sintering", *Industrial and Engineering Chemistry Research*, Vol. 38, pp. 3868–3872, 1999.

55. Nie, Z.-g. and D.-y. Fang, "Global Kinetics of Direct Synthesis of Dimethyl Ether from Syngas Containing N˜ 2 over Bifunctional Mixed Catalyst", *Journal East China University of Science and Technology*, Vol. 30, No. 4, pp. 370–374, 2004.

56. Mei, D., L. Liang, M. Qian and X. Lou, "Modeling and analysis of flow distribution in an A-type microchannel reactor", *International Journal of Hydrogen Energy*, Vol. 38, No. 35, pp. 15488 – 15499, 2013.

57. Portha, J. F., K. Parkhomenko, K. Kobl, A. Roger, S. Arab, J. M. Commenge and L. Falk, "Kinetics of methanol synthesis from carbon dioxide hydrogenation over copper–zinc oxide catalysts", *Industrial and Engineering Chemistry Research*, Vol. 56, pp. 13133–13145, 2017.

58. Tezcan, I. and A. K. Avcı, "Parametric investigation of oxidative coupling of methane in a heat-exchange integrated microchannel reactor", *Journal of Chemical Technology and Biotechnology*, Vol. 90, pp. 1827–1838, 2015.

59. Karakaya, M. and A. K. Avcı, "Simulation of on-Board Fuel Conversion in Catalytic Microchannel Reactor-Heat Exchanger Systems", *Topics in Catalysis*, Vol. 52, pp. 2112–2116, 2009.

60. Veser, G. and J. Frauhammer, "Modelling steady state and ignition during catalytic methane oxidation in a monolith reactor", *Chemical Engineering Science*, Vol. 55, pp. 2271–2286, 2000.

61. Avcı, A. K., D. L. Trimm and M. Karakaya, "Microreactor catalytic combustion for chemicals processing", *Catalysis Today*, Vol. 155, pp. 66–74, 2010.

62. Onsan, Z. I. and A. K. Avcı, *Multiphase Catalytic Reactors: Theory, Design, Manufacturing, and Applications*, Wiley, Haboken, 2016.

63. Avci, A., D. Trimm and Z. İlsen Önsan, "Heterogeneous reactor modeling for simulation of catalytic oxidation and steam reforming of methane", *Chemical Engineering Science*, Vol. 56, No. 2, pp. 641 – 649, 2001, 16th International Conference on Chemical Reactor Engineering.

64. Froment, G. F., K. B. Bischoff and J. De Wilde, *Chemical reactor analysis and design*, Vol. 2, Wiley New York, 1990.